Received: 30 June 2023 | Revised: 25 June 2024 | Accepted: 2 July 2024

DOI: 10.1002/jex2.167

RESEARCH ARTICLE

Optimization of ultracentrifugation-based method to enhance the purity and proteomic profiling depth of plasma-derived extracellular vesicles and particles

Zurong Wan[1,2] | **Jinghua Gu**[1,2] | **Uthra Balaji**[1,2] | **Linda Bojmar**[3,4] | **Henrik Molina**[5] | **Søren Heissel**[5] | **Alexandra E. Pagano**[5] | **Christopher Peralta**[5] | **Lee Shaashua**[3] | **Dorina Ismailgeci**[6] | **Hope K. Narozniak**[6] | **Yi Song**[7] | **William R. Jarnagin**[7] | **David P. Kelsen**[6] | **Jaqueline Bromberg**[6,8] | **Virginia Pascual**[1,2] | **Haiying Zhang**[3]

[1]Drukier Institute of Children's Health, Weill Cornell Medicine, New York, New York, USA

[2]Department of Pediatrics, Weill Cornell Medicine, New York, New York, USA

[3]Children's Cancer and Blood Foundation Laboratories, Departments of Pediatrics, and Cell and Developmental Biology, Meyer Cancer Center, Weill Cornell Medicine, New York, New York, USA

[4]Department of Clinical and Experimental Medicine, Linköping University, Linköping, Sweden

[5]Proteomics Resource Center, The Rockefeller University, New York, New York, USA

[6]Department of Medicine, Memorial Sloan Kettering Cancer Center, New York, New York, USA

[7]Hepatopancreatobiliary Service, Department of Surgery, Memorial Sloan Kettering Cancer Center, New York, New York, USA

[8]Department of Medicine, Weill Cornell Medicine, New York, New York, USA

Correspondence
Virginia Pascual, Drukier Institute of Children's Health, Department of Pediatrics, Weill Cornell Medicine, 413 E. 69th Street, Box 284, New York, NY 10021, USA.
Email: vip2021@med.cornell.edu.

Haiying Zhang, Departments of Pediatrics, and Cell and Developmental Biology, Weill Cornell Medicine, 413 E. 69th Street, Box 284, New York, NY 10021, USA. Email: haz2005@med.cornell.edu

Funding information
Hartwell Foundation; Feldstein Medical Foundation; Sohn Conferences Foundation; Manning Foundation; National Cancer Institute, Grant/Award Numbers: CA169538, CA210240, CA207983, CA218513, CA232093, CA163117, CA224175, CA163120; the Leona M. and Harry B. Helmsley Charitable Trust; Thompson Family Foundation; Theodore A. Rapp Foundation; Alex's Lemonade Stand Foundation; Swedish Cancer Society project grant, Grant/Award Number: 21 1824 Pj 01 H; Tortolani Foundation; Breast Cancer Research Foundation; Drukier Institute for Children's Health at Weill Cornell Medicine; Swedish Society for Medical Research, Grant/Award Number: S21-0079; Sohn Foundation; Malcolm Hewitt Weiner Foundation;

Abstract

Circulating extracellular vesicles and particles (EVPs) are being investigated as potential biomarkers for early cancer detection, prognosis, and disease monitoring. However, the suboptimal purity of EVPs isolated from peripheral blood plasma has posed a challenge of in-depth analysis of the EVP proteome. Here, we compared the effectiveness of different methods for isolating EVPs from healthy donor plasma, including ultracentrifugation (UC)-based protocols, phosphatidylserine-Tim4 interaction-based affinity capture (referred to as "PS"), and several commercial kits. Modified UC methods with an additional UC washing or size exclusion chromatography step substantially improved EVP purity and enabled the detection of additional proteins via proteomic mass spectrometry, including many plasma membrane and cytoplasmic proteins involved in vesicular regulation pathways. This improved performance was reproduced in cancer patient plasma specimens, resulting in the identification of a greater number of differentially expressed EVP proteins, thus expanding the range of potential biomarker candidates. However, PS and other commercial kits did not outperform UC-based methods in improving plasma EVP purity. PS yielded abundant contaminating proteins and a biased enrichment for specific EVP subsets, thus unsuitable for proteomic profiling of plasma EVPs. Therefore, we have optimized UC-based protocols for circulating EVP isolation, which enable further in-depth proteomic analysis for biomarker discovery.

AHEPA Vth District Cancer Research Foundation; Daedalus Fund Selma and Lawrence Ruben Science to Industry Bridge Award; Swedish Research Society Starting Grant, Grant/Award Number: 2021-02356; National Institute of Allergy and Infectious Diseases, Grant/Award Number: AI144301; Pediatric Oncology Experimental Therapeutics Investigator's Consortium; Children's Cancer and Blood Foundation

KEYWORDS
biomarkers, early cancer detection, extracellular vesicles and particles (EVPs), proteomics

1 | INTRODUCTION

In the past decade, circulating extracellular vesicles (nanoparticles enclosed by a lipid bilayer, such as exosomes) and particles (nanoparticles lacking external membranous structure, such as exomeres) (EVPs) have emerged as promising biomarker reservoirs for early cancer detection, prognosis, and monitoring treatment response in cancer patients (Chen et al., 2017; Hoshino et al., 2015, 2020; Lucotti et al., 2022; Shimada et al., 2021). Tumor cells actively release EVPs to mediate intercellular communication with cells in the local tumor microenvironment as well as with cells in distant organs, including pre-metastatic niches at future sites of metastasis, through circulation (Lucotti et al., 2022; Pelissier Vatter et al., 2021; Sheehan & D'Souza-Schorey, 2019; Xu et al., 2018). Tumor-derived EVPs are released in peripheral blood and hold high potential for identifying biomarkers in minimally invasive liquid biopsies for cancer patients (Colombo et al., 2014; Fraser et al., 2019). In addition to EVPs shed by tumor cells, EVPs are also produced by cells in the tumor microenvironment as well as cells in distant organs that have been systemically influenced by the tumor. These EVPs can also contribute to biomarker reservoirs reflective of disease status. For example, alterations in the protein cargos of EVPs released from a perturbed immune system in cancer patients can be detected in the circulating EVP pool and used to distinguish cancer patients from healthy donor (HD) controls (Hoshino et al., 2020).

An essential step in identifying novel circulating EVP-based biomarkers is to perform an in-depth characterization of the molecular cargos carried by EVPs in plasma. Besides cataloging EVP-associated RNAs (especially microRNAs), proteomic profiling of plasma EVPs via mass spectrometry (MS) has emerged as a predominant strategy for biomarker discovery (Choi et al., 2015; Ko et al., 2018). We recently conducted a comprehensive proteomics study in which we identified EVP-based biomarkers for cancer detection in multiple cancer types (Hoshino et al., 2020). Despite the success of this study, we observed that the plasma-derived EVPs isolated using the same differential ultracentrifugation (UC) method, involving two steps of high-speed UC, yielded a much lower total number of different proteins identified compared to EVPs derived from cell lines and tissue explant cultures. For example, an average of 265 proteins were identified via proteomic MS in plasma EVPs whereas an average of 852 and 1482 proteins were identified in EVPs isolated from human cell lines and tissue explant cultures, respectively. We reasoned that the lower detection rates for plasma-derived EVP samples were likely due to the high abundance of contaminants uniquely present in these samples but not EVPs isolated from other sources. Therefore, we aimed to optimize our current EVP isolation procedure further to enhance the purity of plasma-derived EVPs and enable more extensive analysis of their proteomes for the discovery of novel biomarkers.

In this work, we compared the performance of several UC-based EVP isolation protocols, the phosphatidylserine-Tim4 interaction-based affinity capture approach (referred as "PS") and several commercial kits. Given the additional contribution of non-tumor tissue-derived EVPs that also reflect the disease status in cancer patients (Hoshino et al., 2020), we thereby focused on EVP isolation procedures that have been developed based on general biophysical properties of EVPs, such as UC-based approaches, rather than immunoaffinity capturing (IAC) approaches that reply on the expression of tumor-specific markers (e.g., EpCAM). Considering EVP heterogeneity and the lack of universal expression of surface markers such as CD9, CD81, and CD63, and especially their absence in exomeres, IAC approaches that rely on the expression of EVP surface markers were not chosen in this study. As phosphatidylserine is a common component of EV membranes and has also been reported in exomeres (although its configuration has not yet been resolved) (Zhang et al., 2018), we sought to compare the PS kit with conventional UC-based methods for isolating EVPs to perform downstream proteomic profiling via MS. Moreover, we also included several commercial kits that enable isolation of EVPs without any limitation to specific EVP subsets for comparison of their performance. We evaluated EVP yield, purity, and the depth of EVP proteome profiling via MS and showed that by adding an additional UC washing step or a size exclusion chromatography step, the optimized UC-based procedures yielded better performance than the other methods assessed in this study.

2 | MATERIALS AND METHODS

2.1 | Plasma samples

Large volume (about 300 mL) of plasma samples from a total of six HDs were purchased from New York Blood Center for method development and comparison (collected using citrate-phosphate-dextrose as anti-coagulant). For the validation study, five patients with newly diagnosed, stage I–III pancreatic cancer and five matching healthy controls were recruited at Memorial Sloan Kettering Cancer Center, and 5–10 mL of blood samples were collected in EDTA tubes (MSKCC, IRB #15-015, IRB # 17–527). Plasma was then prepared by 10 min centrifugation at 500×*g*, 20 min centrifugation at 3000×*g*, and the supernatant was collected and stored at −80°C for EVP isolation. All individuals provided informed consent for sample collection according to protocols approved by the Institutional Review Boards of MSKCC and NIH. The study is compliant with all relevant ethical regulations regarding research involving human participants.

2.2 | Purification of EVPs

Plasma samples were thawed at 4°C and centrifuged at 12,000×*g* for 20 min at 10°C to remove large microvesicles. Supernatant was then transferred to new tubes (Beckman Coulter, 355645) and centrifuged at 100,000×*g* for 70 min at 10°C using 50.4Ti rotor (Beckman Coulter, 347299) in a Beckman Coulter Optima XE or XPE ultracentrifuge. Pellets were re-suspended in ice-cold PBS, and at least 2 mL of PBS was used to wash each sample. Samples were centrifuged again at 100,000×*g* for 70 min at 10°C. For UC2, the pellets were re-suspended in 150 µL of PBS. For UC3, the pellets were re-suspended in 2 mL of ice-cold PBS and another round of centrifugation was performed at 100,000×*g* for 70 min at 10°C. The pellets were re-suspended in 150 µL of PBS. To obtain enough EVP products for a range of downstream assays, we typically initiate with 5 mL of plasma for UC2, 8 mL for UC3, and up to 40 mL for UC2-qEV.

For UC2-qEV, EVPs purified by UC2 were re-suspended in 500 µL of PBS and loaded onto qEV original/70 nm (Izon, ICO-70) columns which were previously equilibrated with 30 mL of ice-cold PBS per manufacture's instruction. The void volume (~3 mL) was discarded, and fractions (0.5 mL per fraction) were collected starting from fraction 7 using the automatic fraction collector (Izon). Fractions 8–10 were EVPs enriched, combined, and concentrated using centrifugal filter units (Millipore, UFC903008) for downstream analysis.

MagCapture Exosome Isolation Kit PS (FUJIFILM Wako Pure Chemical Corporation, 293–77601) was used for PS beads-based isolation of EVPs. One milliliter of plasma was centrifuged at 12,000×*g* for 20 min at 10°C, and the supernatant was used for each purification following essentially the manufacturer's protocol.

For qEV-DGC, 0.5 mL of plasma was applied to the qEV column as described above and EVP-containing fractions from five runs were pooled and concentrated using centrifugal filter units (Millipore, UFC903008) and diluted with PBS to a final volume of 500 µL. To prepare the discontinuous iodixanol gradient, 40% (w/v), 20% (w/v), 10% (w/v), 5% (w/v) solutions of iodixanol were made by diluting OptiPrep (Cosmo Bio, AXS-1114542) (60% (w/v)) with sucrose solution (0.25 M, 10 mM Tris, pH 7.5). To set the gradient, 3 mL of 40% iodixanol solution was added to the bottom of a 14 × 95 mm ultra clear tube (Beckman Coulter, 344060). 3 mL of 20% solution was gently layered to the top of 40% solution with a syringe, followed by 3 mL of 10% solution and 2.5 mL of 5% solution. 500 μL of concentrated qEV eluate were overlaid onto the top of the gradient. The gradient was centrifuged at 100,000 x g for 16 h at 10°C using a SW-40Ti rotor (Beckman Coulter, 331302). 12 fractions of 1 mL were collected with pipettes from top to bottom. Fractions 6-9, which were enriched for EVPs, were pooled, diluted with 11 mL of PBS, and concentrated using centrifugal filter units (Millipore, UFC903008).

For DGC+Bind-Elute size exclusion chromatography (BE-SEC), the discontinuous iodixanol gradient was prepared as described previously. Plasma was centrifuged at 12,000 x g for 20 min, and 500 μL of supernatant was overlaid onto the top of each gradient. The gradient was centrifuged at 100,000×*g* for 16 h at 10°C using a SW-40Ti rotor (Beckman Coulter, 331302). Twelve fractions of 1 mL were collected with pipettes from top to bottom. Fractions 6–9 from four gradients (2 mL plasma total) were pooled, diluted with PBS, and concentrated using centrifugal filter units (Millipore, UFC9030). The concentrated EVP sample was further washed with 11 mL of PBS and concentrated using centrifugal filter units twice. A HiScreen Capto Core 700 column (4.7 mL bed volume, Cytiva, 17548115) was connected and run using the AKTAPure system, and a HiTrap Capto Core 700 column (1 mL bed volume, Cytiva, 17548151) was connected to a syringe and operated manually according to the manufacturer's instructions. The columns were washed with distilled water first and then equilibrated with five column volumes of PBS. The concentrated EVP samples were then loaded onto the columns and eluted with PBS. The flow rate was 1 mL/min for the HiScreen column and approximately 1.8 mL/min for the HiTrap column. Fractions were collected and concentrated using centrifugal filter units (Millipore, UFC5030) for BCA quantification, ELISA and EM imaging analysis. Cleaning-In-Place (CIP) was performed according to the manufacturer's manual to recover the columns for future use. EVP-containing fractions, as revealed by CD9 ELISA, were further combined for Western blot analyses.

Four commercial kits were also used for EVP purification: exoEasy Maxi Kit (Qiagen, 76064); Exo-spin midi (Cell Guidance Systems, EX04-5); ExoQuick Exosome Isolation and RNA Purification Kit (for Serum & Plasma) (System Biosciences, EQ806A-1); and miRCURY Exosome Serum/Plasma Kit (Qiagen, 76603). EVP purification was performed following the manufacturer's instructions, and EVPs were re-suspended in PBS.

2.3 | EVP characterization

BCA Protein Assay (Pierce, Thermo Fisher Scientific, 23227) and Nanosight Tracking Analysis (NTA) were conducted upon isolated EVPs following manufacturer's manual for protein quantification and particle size and number measurement, respectively. NS500 nanoparticle characterization system (NanoSight, Malvern Instruments) equipped with a blue laser (405 nm) was utilized for NTA. PS Capture Exosome ELISA Kit (Anti Mouse IgG POD) (FUJIFILM Wako Pure Chemical Corporation, 297–79201) was utilized to evaluate the relative purity of isolated EVPs and recovery rate from plasma. The Nalm6 cell line-derived EVPs purified by UC2 were used as ELISA standards. Five hundred nanogram of Nalm6 EVPs in 200 μL of PBS was used as the first standard sample, from which the following six standard samples were prepared by serial dilution. The detecting antibody recognizes the CD9 antigen (HI9a). The relative purity of EVPs isolated using each protocol was expressed as the ratio of purified EVP amount (estimated by ELISA) to total protein amount (determined by BCA). Recovery rate was calculated as the ratio of purified EVP amount to the total EVP amount present in the input plasma (both evaluated by ELISA).

2.4 | Western blotting

EVPs were first lysed in SDS lysis buffer (Biorad, #1610772EDU). EVPs isolated from an indicated volume of plasma were diluted with reducing sample buffer (Biorad, #1610747), separated on Novex 4%−20% Tris-glycine gels (Life Technologies, XP04122BOX) and transferred onto polyvinylidene difluoride membranes (Biorad, #1704273). Membranes were sequentially blocked with 1X TBS containing 5% non-fat milk (w/v) and 0.1% Tween20 (v/v), incubated with primary antibodies overnight at 4°C, rinsed three times and washed four times with 1X PBS containing 0.1% Tween20 (v/v), incubated with secondary antibodies (horseradish peroxidase-conjugated anti-mouse (invitrogen, G-21040) or anti-rabbit (CST, 7074P2) and washed again to remove unbound antibodies. Bound antibody complexes were detected with SuperSignal West Pico Chemiluminescent Substrate (Thermo Fisher, 34078) or SuperSignal West Femto Maximum Sensitivity Substrate (Thermo Fisher, 34095) and visualized using the Bio-Rad ChemiDoc Touch Imaging System. The primary antibodies used for western blotting include: anti-Apo AI (Abcam, ab64308); anti-HSA (Abcam, ab10241); Peroxidase AffiniPure Goat Anti-Human IgG (Jackson Immunoresearch, 109-035-190); anti-Flotillin-1(BD, 610820); anti-Hsp90 (Invitrogen, MA5-15863); anti-CD9 (Abcam, ab223052); and anti-Syntenin-1 (Santa Cruz, sc-100336). The signal intensity of bands was quantified using ImageJ. After subtracting the background, intensity value of each band was normalized against the mean intensity of UC2 samples of the same experiment.

2.5 | TEM

Negative staining TEM analysis was performed as previously described (Zhang et al., 2018). In brief, 5 μL of EVPs (0.1 μg/μL in PBS) isolated using different methods (EVPs isolated using PS in a concentration less than 0.1 μg/μL in Elution Buffer provided by the kit) were placed on a formvar/carbon-coated grid and allowed to settle for 1 min. The sample was then blotted and negatively stained with four successive drops of 1.5% aqueous uranyl acetate, blotting between each drop. Grids were air-dried and imaged with a JEOL JSM 1400 (JEOL, USA, Ltd, Peabody, MA) transmission electron microscope operating at 100 kV. Images were captured on a Veleta 2k × 2k charge-coupled device camera (Olympus-SIS, Munich, Germany).

2.6 | Proteomic mass spectrometry

Proteomic MS and database search were performed as previously described (Zhang et al., 2018). In brief, 2 μg of isolated EVP samples were vacuum-dried and re-dissolved in 30–50 μL of 8 M Urea/50 mM ammonium bicarbonate/10 mm DTT. Proteins were then alkylated using 20 or 30 mM iodoacetamide (Sigma) and digested with Endopeptidase Lys C (Wako) in <4 M urea followed by trypsination (Promega) in <2 M urea. Peptides were desalted and concentrated using Empore C18-based solid phase extraction. Peptides were separated using a high resolution/high mass accuracy reversed phase C18 column (12 cm/75 mm, 3 mm beads, Nikkyo Technologies) at 200 or 300 nL/min with a gradient increasing from 1% Buffer B/95% buffer A to 40% buffer B/60% Buffer A in typically 90 or 120 min (buffer A: 0.1% formic acid, buffer B: 0.1% formic acid in 80% acetonitrile). Typically, 1.875 μg

of samples were injected. Mass spectrometer (Fusion Lumos, Thermo Scientific) was operated in data dependent (DDA) positive ion mode.

Proteome Discoverer 1.4.1.14 (Thermo-Scientific, 2012)/Mascot 2.5 (Perkins et al., 1999) was used for processing the high resolution/high mass accuracy nano-LC-MS/MS data. Human data were queried against the UniProt's Complete HUMAN proteome (February, 2020:74,788 sequences) using the following parameters: Enzyme: Trypsin/P; maximum allowed missed cleavage sites: 2; monoisotopic precursor mass tolerance:10 ppm; monoisotopic fragment mass tolerance: 0.02 Da; dynamic modifications: Oxidation (M), Acetyl (Protein N-term); static modification: Carbamidomethyl (C). Percolator was used to calculate peptide false discovery rates (FDR), which were calculated per file. An FDR of 1% was applied to each separate LC-MS/MS file. The sequences of porcine trypsin and Endopeptidase LysC were concatenated to the human databases.

2.7 | Bioinformatics

For mass spectrometry proteomics data analysis, R (R Core Team, 2021) package DEP (Zhang et al., 2018) was used for the processing of proteomics data. Briefly, data were first filtered, background-corrected and normalized, and imputed for missing values. Principal component analysis (PCA) was performed, and the first two principal components were used to visualize the proteomics data and evaluate global differences between technical groups. Batch effect was observed between multiple MS runs and was corrected using the removeBatchEffect function from the limma package (Ritchie et al., 2015) before plotting PCA and heatmaps.

Differentially detected proteins were identified based on filtered, background-corrected and normalized, and imputed data using functions from the limma package. Batch effect was included in the linear model fitted by the lmFit function. Within-donor correlation was calculated using the duplicateCorrelation function. Log fold-changes between groups were obtained by makeContrasts function, and contrast was estimated for each gene by contrasts.fit function. Empirical Bayes smoothing of standard errors was performed, and proteins that showed at least a log fold change of 1.5 and an adjusted p value of <0.05 were considered differentially expressed. Heatmaps were created using heatmap.2 function from gplots package.

Gene set enrichment analysis (GSEA) was done using javaGSEA through the Broad Institute. For each comparison, all proteins were ranked by t-statistic and preranked analysis was used to look at enrichment in top 200 proteins originally detected in human plasma by MS (human protein atlas: https://www.proteinatlas.org/humanproteome/blood+protein/proteins+detected+in+ms), and ECM-associated proteins (MatrisomeDB) (https://matrisomedb.org). The default parameters were used in all analyses.

Subcellular localization of proteins was determined by QIAGEN Ingenuity Pathway Analysis (QIAGEN IPA). Pathway analysis and tissue- and cell type-specific origin analysis were performed using the web-based Metascape resource platform.

The MS-based proteomics raw data have been deposited to the ProteomeXchange Consortium via the PRIDE partner repository (https://www.ebi.ac.uk/pride) and is available via ProteomeXchange with identifier PXD052726. The proteomics datasets have also been deposited in the Figshare repository. Specifically, the proteomics data pertaining to the comparison of various methods, including UC2, UC3, UC2-qEV, and PS, can be accessed at the following https://doi.org/10.6084/m9.figshare.22798619. The proteomics data comparing qEV-DGC and UC are available at DOI: https://doi.org/10.6084/m9.figshare.22798934. Lastly, the proteomics data related to plasma EVP samples from pancreatic cancer patients and healthy controls can be found at https://doi.org/10.6084/m9.figshare.22798940.

2.8 | Statistical analysis

To determine statistical significance for assays including BCA, NTA, WB and ELISA, one-way ANOVA with Geisser-Greenhouse correction, in accordance with recommended guidelines for within-subjects analysis, was used, followed with Bonferroni's multiple comparisons test (GraphPad). For identification of differentially detected proteins via mass spectrometry, we incorporated within-donor correlation by utilizing the duplicateCorrelation function. As a result, these analyses were systematically conducted in a pairwise manner. p value < 0.05 was considered statistically significant. $^{*}p < 0.05$, $^{**}p < 0.01$, $^{***}p < 0.001$, $^{****}p < 0.0001$.

3 | RESULTS

3.1 | Establishing protocols to isolate plasma EVPs with improved purity

To establish and compare different protocols for EVP isolation from plasma, large volumes of plasma from HDs (purchased from New York Blood Center) were used unless specified otherwise. This allowed us to compare the performance of different protocols using the same specimen, thereby avoiding confounding effects from individual variance. The differential UC protocol, one of the most well-established and commonly used protocols in the field, involves two sequential steps of UC at 100,000 g (referred to as

"UC2") and was included as a reference for performance comparison of EVP isolation procedures (Figure 1a). To improve purity, EVPs isolated via UC2 were either subjected to a third UC step (referred to as "UC3") or loaded onto a size-exclusion column (referred to as "UC2-qEV"). The MagCapture Exosome Isolation Kit PS (FUJIFILM Wako Pure Chemical Corporation, referred to as "PS") employing the interaction between Tim4 and phosphatidylserine present on the surface of EVPs was compared in parallel. To acquire an ample quantity of EVP products for a range of downstream assays, we typically initiate with 5 mL of plasma for UC2, 8 mL for UC3, up to 40 mL for UC2-qEV, and 1 mL for PS. BCA assay, Nanoparticle Tracking Analysis (NTA), negative staining transmission electron microscopy (TEM) and Western blotting (WB) analysis were conducted to evaluate the yield and purity of EVP samples isolated through these four protocols.

The protein concentration of isolated EVPs was determined by BCA assay and then standardized to a unit volume of plasma, serving as a reference. UC2 yielded the highest number of proteins (12 μg/mL) on average, followed by PS (7 μg/mL plasma), UC3 (3 μg/mL), and UC2-qEV (0.4 μg/mL) (Figure 1b). The particle size and number were determined by NTA (Figure 1c). The size of particles isolated through different protocols was quite similar, with UC3 EVPs being marginally larger and UC2-qEV EVPs slightly smaller than PS and UC2 EVPs. PS and UC2 yielded similar numbers of particles per unit volume (mL) of plasma, while UC2-qEV yielded a significantly lower number of particles per mL of plasma (p value = 0.047). UC3 showed a trend toward lower yield though not statistically significant (p value = 0.083). In contrast, when we normalized particle number to total protein amount, we found that UC2-qEV ranked highest (p value = 0.0001), followed by UC3, PS, and UC2. It should be noted that the detection range of NTA is limited to particles down to 60–70 nm (Zhang et al., 2018), therefore the small extracellular vesicles and exomeres below 60 nm in size cannot be measured accurately by this method. Additionally, NTA is not able to distinguish between EVPs and other particles such as chylomicrons and very low-density lipoproteins (VLDL) due to their overlap in size.

Next, we examined the morphology and purity of the isolated EVPs by conducting negative staining TEM analysis (Figure 1d). The size range and morphology of EVPs isolated through all four protocols are comparable. Nonetheless, with equivalent or even less protein loaded, we observed more membranous vesicle structures (marked by red arrows) in images of EVPs isolated through UC3, UC2-qEV and PS compared to UC2. Compared to the dark background of UC2 and PS images, likely due to the presence of highly abundant plasma proteins (the contaminants), the images of EVPs isolated through UC2-qEV, and to a less extent UC3, showed fewer background contaminants, indicating an improvement in EVP purity. Due to the physical property overlap between lipoprotein particles and EVPs and the higher abundance of lipoproteins in blood (10^{13}–10^{16} /mL of blood depending on lipoprotein type (Simonsen, 2017) versus 10^{7}–10^{9}/mL for EVPs (Arraud et al., 2014)), lipoproteins are a major contaminant in plasma-derived EVPs. Indeed, we observed that the number of bright, bubble-like structures (examples marked by black arrows), which resemble lipoprotein nanoparticles, are reduced in EVPs isolated through UC3 and UC2-qEV compared to UC2. In contrast, the PS kit enriched for such structures alongside EVPs, which can be explained by a previous study reporting enrichment of PS in a subset of high-density lipoproteins (HDL) (Camont et al., 2013).

To evaluate the yield and purity of these EVP samples, we performed WB analysis for four well-documented EVP markers (i.e., heat shock protein 90/Hsp90, Flotillin-1/Flot-1, Syntenin-1/SDCBP and tetraspanin CD9) as well as three plasma soluble proteins (i.e., human serum albumin/HSA, immunoglobulin G/IgG and apolipoprotein AI/ApoAI) that are potential contaminants. The loading volume for each group (as indicated on top of Figure 1e) was established so most bands were visible and quantifiable. To compare the yield, the abundance of EVP markers was first normalized to the starting volume of plasma (Figure 1f). Our results showed that among the four protocols tested, UC2-qEV followed by UC3 had the lowest yield of all four tested EVP markers. UC2 protocol recovered higher levels of Hsp90 and SDCBP than other protocols, while the PS kit enriched most for Flot-1 and CD9. The decrease in the levels of HSA, IgG and ApoAI in EVPs isolated using UC3 and UC2-qEV, compared to UC2, was more significant than the decrease in the levels of EVP markers, indicating improved EVP purity with UC3 and UC2-qEV (see below). In contrast, PS retained relatively high levels of HSA, IgG and ApoAI contaminants with large individual variance.

To compare the EVP purity, the abundance of the examined proteins was normalized to the amount of total protein (Figure 1g). The highest enrichment of the four EVP markers was observed in samples prepared by UC2-qEV followed by UC3. Intriguingly, the PS kit enriched for Flot-1, and to a less extent CD9, but not SDCBP or Hsp90. Although HSA was significantly depleted by UC3 and UC2-qEV, the relative abundance of IgG and ApoAI was not significantly changed in EVPs isolated through all four protocols. Notably, the different levels of enrichment of extracellular vesicle markers (Flot-1, SDCBP and CD9) by the PS kit underscore the heterogeneity of EVPs and implicates enrichment of specific EVP subsets (e.g., Flot-1-high subsets) using PS.

In summary, the BCA, NTA, WB, and TEM analyses collectively demonstrate that EVPs isolated using UC2-qEV and UC3, as compared to UC2, exhibit higher purity but lower yield, whereas the PS kit provides a comparable yield but with a biased enrichment for specific EVP subsets and poor purity.

3.2 | Performance evaluation of commercial kits for plasma EVP isolation compared to UC-based approaches

Several commercial kits for EVP isolation offer convenience by eliminating specific equipment requirements, including an ultra-centrifuge. However, their suitability for isolating EVPs from plasma and downstream proteomic profiling has not been evaluated

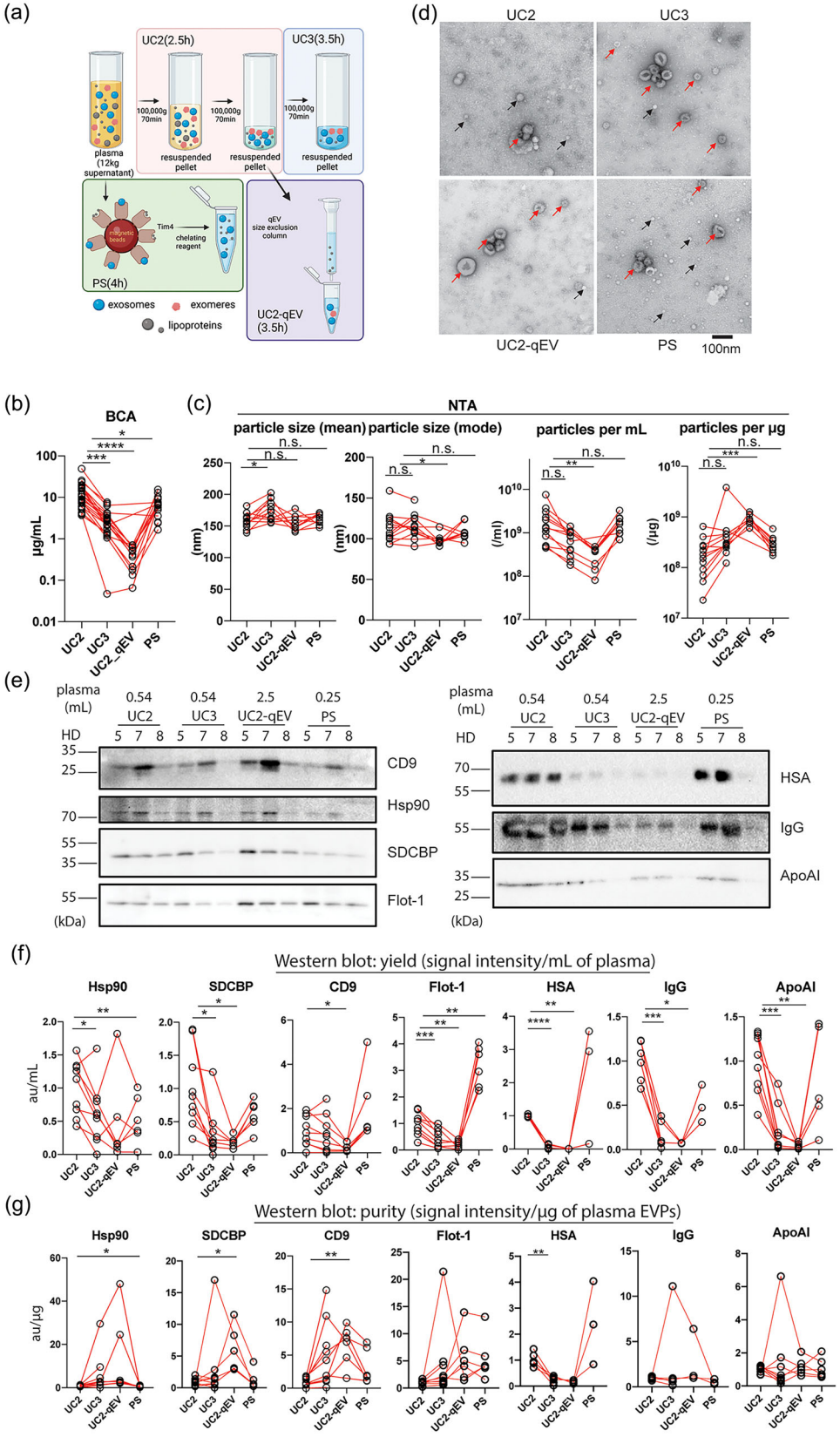

FIGURE 1 Establishment and performance comparison of protocols for isolating plasma EVPs with improved purity. (a). Diagrams illustrating the four major procedures compared for performance for isolating plasma EVPs. Estimated execution time for each procedure is listed in parenthesis. Other methods examined but not illustrated in this figure include qEV-DGC (size exclusion chromatography followed by density gradient ultracentrifugation), DGC+BE-SEC (DGC followed by bind-elute size exclusion chromatography),exoEasy Maxi Kit (Qiagen), Exo-spin midi (Cell Guidance Systems), ExoQuick Exosome Isolation and RNA Purification Kit (for Serum & Plasma) (System Biosciences), and miRCURY Exosome Serum/Plasma Kit (Qiagen). (b). Quantification of

(Continues)

FIGURE 1 (Continued)

total protein yield in isolated plasma EVPs using BCA assay. $n >= 12$. (c) Assessment of particle size (mode and mean) and number (per mL of plasma input and per μg of isolated EVPs) in isolated plasma EVPs using Nanoparticle Tracking Analysis (NTA). $n >= 8$. (d) Representative TEM images of plasma EVPs isolated using different approaches. Red and black arrows indicate EVPs and particles resembling lipoprotein nanoparticles. Scale bar, 100 nm. (e) Western blotting (WB) analysis of EVP marker proteins and potential contaminants in plasma EVPs isolated from three healthy donors (HD). The volume of input plasma analyzed for each sample is indicated on top of the images. CD9, Tetraspanin CD9; Hsp90, Heat shock protein 90; SDCBP, Syntenin-1; Flot-1, Flotillin-1; HSA, Human serum albumin; IgG, Immunoglobulin G; and ApoAI, Apolipoprotein AI. f and g. Quantification of WB analysis results to evaluate the yield (expressed as EVP marker protein signal/mL of plasma) and purity (expressed as EVP marker protein or contaminant signal/μg of EVPs) of isolated plasma EVPs, respectively. $n >= 3$. In all graphs, the bar indicates mean. One-way ANOVA with Geisser-Greenhouse correction was used, followed with Bonferroni's multiple comparisons test to determine the statistical significance.

in comparison to the UC-based approaches. Therefore, in this study, we compared the performance of four commercially available EVP isolation kits, that is, exoEasy Maxi Kit (1.5 mL of plasma was processed), Exo-spin midi (1 mL of plasma was processed), ExoQuick Exosome Isolation and RNA Purification Kit (for Serum and Plasma, 0.5 mL of plasma was processed), and miRCURY Exosome Serum/Plasma Kit (0.6 mL of plasma was processed), with UC2 and UC3 as described above, in terms of EVP purity. Given that the UC2-qEV protocol requires a significantly larger quantity of plasma as the starting material, we opted not to include it in this comparison.

We first used the PS ELISA assay to evaluate the EVP isolation efficiency of these commercial kits in comparison to the UC-based methods. PS^+ EVPs were captured using Tim-4 and detected using antibodies against CD9, one of the most frequently detected markers on plasma EVPs (Hoshino et al., 2020). Although CD9 and PS expressing EVPs may represent only a subset of the plasma EVPs, we used the isolation efficiency of this subset as an indicator of overall EVP isolation efficiency. By calculating the ratio of CD9 abundance in the purified EVPs to the CD9 abundance in the original plasma input, we found that three out of the four kits (excluding exoEasy Maxi Kit) retained the majority of $CD9^+$ EVPs and their isolation efficiency was significantly higher than that of the UC2 and UC3 (Figure S1a). However, when the CD9 abundance was normalized to the amount of the final EVP product, we found that the relative purity of $CD9^+$ EVPs was two (Exo-spin midi) or three (exoEasy Maxi Kit, ExoQuick Exosome Isolation and RNA Purification Kit for Serum & Plasma, and miRCURY Exosome Serum/Plasma Kit) orders of magnitude lower than UC2 and UC3 (Figure S1a). This was consistent with the TEM analysis of these samples (Figure S1b), which appear dominated by a high proportion of contaminants, such as lipoprotein particles and soluble plasma proteins. Based on these observations, we concluded that none of these kits outperformed UC2 and UC3 with respect to the purity of isolated plasma EVPs. Therefore, we did not further explore their utility for downstream proteomic profiling studies.

3.3 | Performance evaluation of density gradient centrifugation in conjugation with size exclusion chromatograph for plasma EVP isolation

Density gradient centrifugation (DGC) is often used for EVP isolation but is labor-intensive and time-consuming (Vergauwen et al., 2021). Here, we compared a two-step protocol combining size exclusion chromatography (SEC) and OptiPrep DGC (referred to as "qEV-DGC", 2.5 mL of plasma was processed) with UC2 and UC3. Given the generally low recovery from the DGC step, we concluded that a single DGC step is practical for most clinical specimens. qEV-DGC is distinct from the UC2-qEV protocol, which is a three-step protocol consisting of two UC steps followed by one SEC step. BCA assay showed that qEV-DGC yielded a larger quantity of proteins than UC2 and UC3 (Figure S1c). The particle size characterized by NTA was comparable among EVPs isolated using UC2, UC3, and qEV-DGC (Figure S1d). When the particle number was normalized to the volume of plasma, qEV-DGC isolated a higher number of particles than UC3 or UC2 (Figure S1d). However, when the particle number was normalized to the protein amount, the qEV-DGC samples showed lower particle numbers per μg of protein than UC2 and UC3 samples, indicating a lower purity of EVPs.

We also conducted CD9 ELISA assay and TEM analysis to evaluate the recovery efficiency and purity of EVPs isolated through qEV-DGC. As shown in Figure S1(a), qEV-DGC resulted in a lower yield and lower purity of CD9 expressing EVPs than UC2 and UC3. Similar observations were made using TEM analysis (Figure S1b).

WB analysis further revealed that qEV-DGC and UC3 had similar yields for the tested EVP markers, HSA and IgG, which were generally lower than UC2 (Figure S1f). However, qEV-DGC resulted in a much higher amount of ApoAI in the isolated EVPs than UC3. When the purity was measured as relative abundance of EVP markers per μg of protein, we found that qEV-DGC and UC2 resulted in comparable enrichment for most EVP markers tested, with a trend lower than UC3 (Figure S1g). Furthermore, qEV-DGC effectively depleted HSA and IgG but not ApoAI from isolated EVPs, indicating significant contamination by HDL. These results indicated that the combination of qEV and DGC did not outperform UC3.

Recently, a modified version of SEC, known as bind-elute size exclusion chromatography (BE-SEC), has been developed and applied to isolate EVPs. BE-SEC technology employs core beads to prevent larger molecules from entering the core, while smaller molecules (<700 kDa) can enter the core and bind to the hydrophobic and positively charged octylamine ligands (cytiva.com)

(Corso et al., 2017). Here, we further assessed the performance of BE-SEC in conjugation with DGC (2 mL of plasma was processed). As shown in Figure S2, CD9+PS+ ELISA and WB analysis of representative EVP markers such as CD9, Flot-1, SDCBP, and Hsp90 indicated a lower yield with DGC+BE-SEC compared to UC2 and UC3. The reduced yield is a limiting factor in this combined method, primarily due to the low recovery from DGC, consistent with our previous testing of the qEV-DGC method. Evaluation based on the CD9+PS+ ELISA, EM, and WB analysis of both EVP markers and common contaminants revealed that the purity of EVPs isolated using the DGC+BE-SEC method is not superior to the UC3 method tested in parallel. Therefore, we did not further pursue the methods involving DGC and SEC in this work. An overall evaluation of the performance of all methods investigated in this study is presented in Figure S3.

3.4 | UC3 and UC2-qEV demonstrate superior performance in enriching exosomes and exomeres and depleting plasma soluble proteins and lipoprotein nanoparticles via proteomic analysis

To examine and compare the proteomes of plasma EVPs purified through different protocols, equal amounts of EVPs isolated from six HDs using each protocol were subjected for proteomic mass spectrometry (MS) analysis in a total of three batches (see details in Figure S4a). First, the number of detected proteins significantly increased in samples prepared through UC3 and UC2-qEV compared to UC2 and PS, with an average of 706 proteins identified by UC2, 1025 proteins by UC3, 1021 proteins by UC2-qEV, and 649 proteins by PS (Figure 2a). This supports our hypothesis that improved EVP purity can enable a deeper, more comprehensive proteomic analysis of EVPs via MS. PCA revealed clustering of samples primarily according to isolating procedures. EVPs prepared through UC2 and PS formed separate clusters, while UC3 and UC2-qEV samples co-mingled (Figure 2b), suggesting a higher degree of similarity.

Next, a closer examination of the proteomes revealed that nearly all the conventional EVP markers (except for CD63) as listed in Figure 2(c) were further enriched using UC3 and UC2-qEV compared to UC2. Intriguingly, PS specifically enriched Flot-1, Flot-2, and HSPA5 but not CD9 and Hsp90 compared to UC2, consistent with the above WB analysis. Other EVP markers, including PDCD6IP/Alix, Tsg101, and CD81, were not enriched by PS compared to UC2. CD63 is unique in that its level was similar across all UC samples but decreased in PS samples. These observations indicate that PS enriches for specific EVP subsets compared to other UC-based procedures.

Soluble proteins that are highly abundant in plasma are considered a significant source of contamination in plasma EVPs. Therefore, we conducted GSEA on the top 200 most abundant proteins identified in human plasma by MS (human protein atlas: https://www.proteinatlas.org/humanproteome/blood+protein/proteins+detected+in+ms). Strikingly, most of these proteins were significantly depleted by UC3 and UC2-qEV compared to UC2 (Figure 2d). However, such a depletion was not observed by PS (Figure 2d). Indeed, we noticed that a subset of plasma proteins was further enriched by PS as shown by the heatmap illustration of their relative abundance in all samples (Figure S4b).

Due to their high abundance and similar size and density to EVPs, lipoprotein particles are another major category of contaminants in EVPs isolated from plasma. Upon close examination of the relative abundance of apolipoproteins in the EVP proteomes, we observed a general trend of apolipoprotein depletion by UC3 and UC2-qEV compared to UC2 (Figure 2e). In contrast, most apolipoproteins were further enriched by PS (Figure 2e), consistent with the TEM and WB analyses described above. These data suggest that PS is less efficient than UC-based approaches in removing lipoprotein particles from EVPs.

Proteomic MS analysis was also performed on EVPs isolated using qEV-DGC as described above (Figure S5). However, no significant enrichment of conventional EVP markers or depletion of top-ranked plasma proteins was observed in EVPs isolated using qEV-DGC compared to UC2, indicating that UC3 and UC2-qEV produced higher quality EVPs for downstream proteomic profiling than qEV-DGC.

3.5 | In-depth characterization of plasma EVP proteomes aided by improved EVP purity

Several classes of proteins of particular interest were further investigated. Integrins (ITGs) are transmembrane proteins present on the surface of exosomes and play important roles in EV biogenesis, targeting, and function in recipient cells (Clayton et al., 2004; Hoshino et al., 2020; Park et al., 2019). Emerging evidence shows that exosomal ITGs represent potential biomarker candidates for disease diagnosis and prognosis (Chen et al., 2021; Hoshino et al., 2020). However, the detection frequency of this family of proteins in plasma EVPs is much lower than in EVPs isolated from cell cultures and tissue explants (Hoshino et al., 2020), thus limiting the exploration of their biomarker potential for liquid biopsies. Our study showed that, compared to UC2, the detection frequency and relative abundance of ITGs were enhanced by UC3 and UC2-qEV but not PS (Figure 2f). This result further supports the necessity of improved EVP purity to facilitate in-depth characterization of the EVP proteomes and subsequent biomarker discovery.

Annexins are another protein family identified as exosomal constituents (Hsu et al., 2021; Keklikoglou et al., 2019; Leoni et al., 2015; Maji et al., 2017; Zhang et al., 2018). A closer examination revealed that almost all annexins detected were significantly

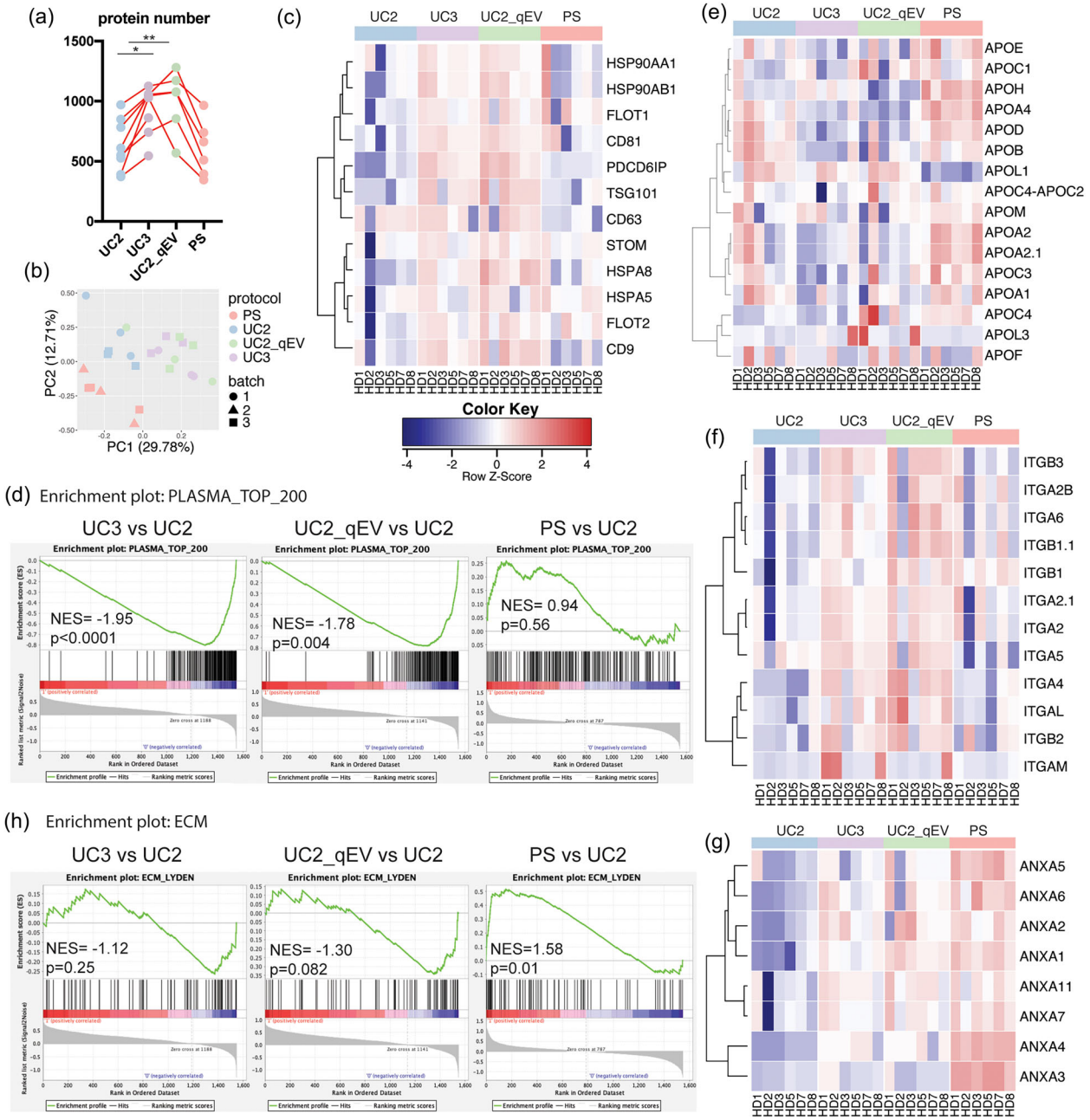

FIGURE 2 Proteomic profiling reveals the enhanced efficiency of UC3 and UC2-qEV in enriching EVPs, while demonstrating biased enrichment of PS. (**a**) Total number of proteins identified in isolated plasma EVPs through proteomic mass spectrometry (MS) analysis. $n = 6$; the bar indicates mean. (b) Principal component analysis of normalized proteomic MS data sets derived from plasma EVPs isolated using different approaches. (c) Heatmap illustration of the relative abundance of conventional EVP marker proteins in plasma EVPs isolated using different approaches. (d) Gene set enrichment analysis (GSEA) illustrating the enrichment or depletion of the top 200-ranked plasma proteins in plasma EVPs isolated using different approaches. (e–g) Heatmap illustration of the relative abundance of apolipoproteins, integrins, and annexins in plasma EVPs isolated using different approaches. $n = 6$ samples per group for (e–g). (h). GSEA of extracellular matrix (ECM)-associated proteins in plasma EVPs isolated using different methods compared to UC2 approach. $n = 6$ samples per group.

enriched in EVPs isolated using PS compared to UC2 (Figure 2g). Such enrichment may be attributed to several factors. Firstly, the binding buffer used in the PS protocol contains Ca^{2+}, which may promote the binding of secreted annexins (such as Annexins A1, A2, and A5) to phosphatidylserine on EVPs. Secondly, annexins may be predominantly located in the inner leaflet of the lipid membrane bilayer of phosphatidylserine^{+} EVs, which could be selectively purified by PS but not by other methods. This finding highlights the potential bias in EVP isolation through PS and its ability to enrich certain EVP subsets carrying specific cargos such as Annexins.

Immunoglobulins constitute a substantial portion of the plasma EVP proteomes, and their differential concentrations in plasma EVP preparations have demonstrated potential for distinguishing cancer from non-cancer or different types of cancers

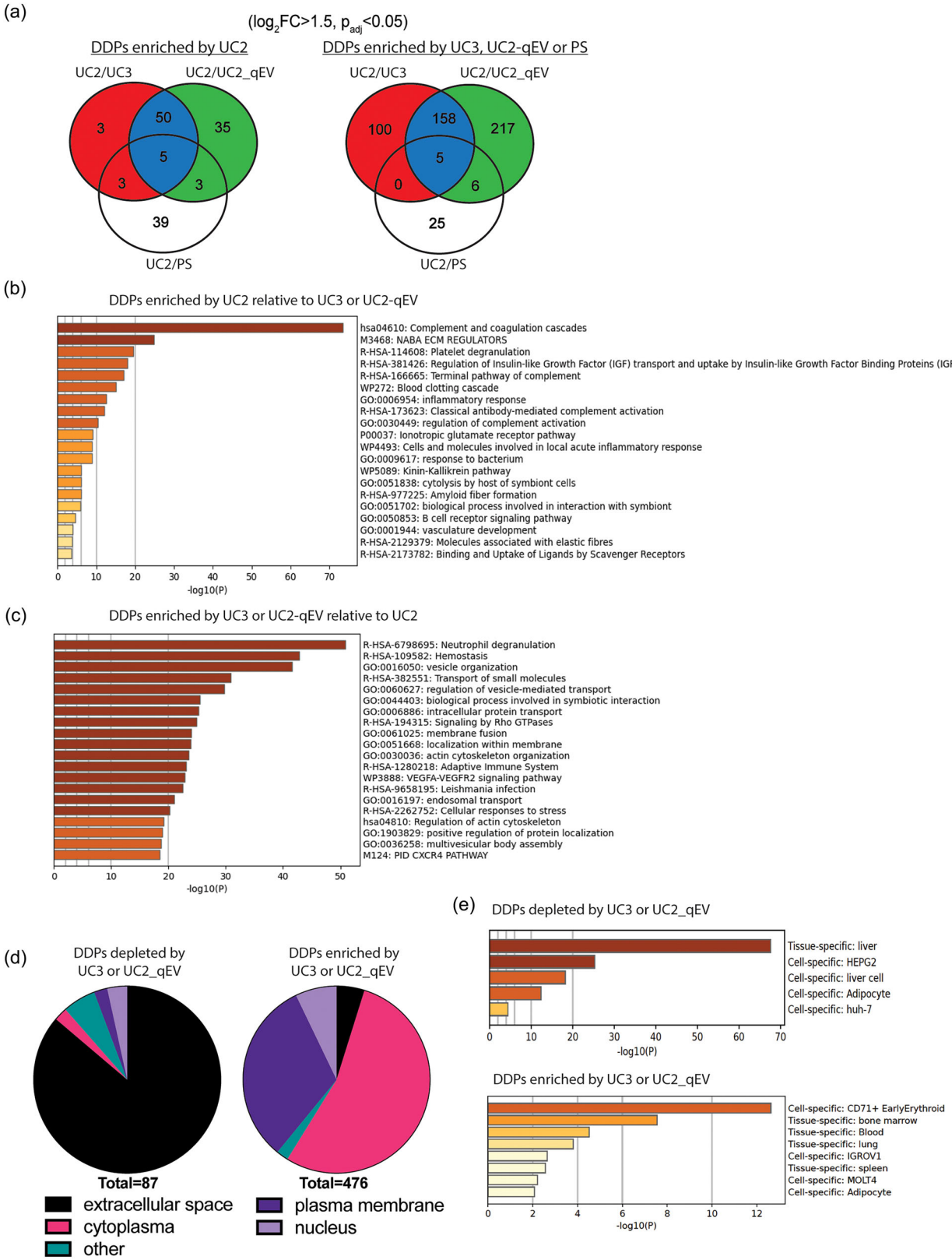

FIGURE 3 Identification and characterization of differentially detected proteins (DDPs) among plasma EVPs isolated using different UC-based approaches. (a) Venn diagrams illustrating differentially expressed proteins in plasma EVPs isolated using UC3, UC2-qEV or PS in comparison with UC2 approach. The criteria for DDP identification include log fold change (FC) > 1.5 and Padj < 0.05. (b, c) Metascape analysis of top pathways associated with DDPs enriched by UC2 (b) or by UC3 or UC2-qEV (c). Statistically enriched ontology clusters are identified through Metascape Express Analysis of ontologies including GO processes, KEGG pathways, Reactome gene sets, canonical pathways, and CORUM complexes. Top non-redundant clusters are presented, with the X-axis illustrating the −log10(*p* value) to convey their statistical significance. (d). Subcellular localization analysis of DDPs depleted (left chart) or enriched

(Continues)

FIGURE 3 (Continued)
(right chart) by UC3 or UC2-qEV in comparison with UC2. (e) Enrichment analysis of tissue- and cell-specific pattern genes in DDPs depleted (top panel) or enriched (bottom panel) by UC3 or UC2-qEV in comparison with UC2. Analysis conducted using PaGenBase through the Metascape online platform.

(Hoshino et al., 2020). Intriguingly, no specific classes of immunoglobulins were greatly enriched by UC3, UC2-qEV or PS compared to UC2 (Figure S6a). In contrast, some of them were either depleted by UC3 and UC2-qEV (including IGHG1, IGHG2, IGHG3 and IGHG4) or by PS (including IGHM, IGKC, IGLC3 and IGLC7), although we observed a significant amount of individual variation among the samples.

Another category of proteins which displayed distinct patterns of enrichment is extracellular matrix (ECM) proteins and ECM-associated proteins. Based on the GSEA and heatmap analysis on the ECM protein set obtained from MatrisomeDB (Figures 2h and S6b), we observed a trend of ECM-associated proteins being depleted by UC3 and UC2-qEV (negative NESs) when compared to UC2. In contrast, there was a strong enrichment of these proteins when using PS (positive NES, $p = 0.01$). For example, we observed a decrease in Fibronectin 1 (FN1), Extracellular Matrix Protein 1 (ECM1), Alpha-1-Microglobulin/Bikunin Precursor (AMBP), and Plasminogen (PLG) in EVPs isolated by UC3 and UC2-qEV compared to UC2, while these proteins were increased in EVPs isolated by PS. In contrast, Transforming Growth Factor-Beta 1 (TGFB1) showed upregulation with UC3 and UC2-qEV but not with PS. Collagen Type VI Alpha chain 2 and 3 (COL6A2 and COL6A3) demonstrated upregulation with all three approaches compared to UC2. The levels of S100 family members (including S100A10, S100A11, S100A6 and S100A4) were slightly higher in samples prepared through UC3 and UC2-qEV than UC2 and PS, while the abundance of S100A9 was comparable across UC3, UC2-qEV and PS samples and higher than that in UC2 samples. Various proteins including Heparan Sulfate Proteoglycan 2 (HSPG2), Microfibril-associated glycoprotein 4 (MFAP4), EGF-containing Fibulin-like Extracellular Matrix Protein 1 (EFEMP1), and Fibulin 5 (FBLN5) were uniquely enriched by PS.

To further assess the efficacy of different methods in enriching EVPs and depleting contaminants, we investigated the signature proteins associated with exosomes and exomeres that we had previously identified in EVPs derived from several cell lines (Zhang et al., 2018). Using UC2 samples as reference, we observed a significant increase in the abundance of exosome and exomere signature proteins in the products of UC2-qEV and UC3, but not in PS (Figure S6c), which is consistent with the aforementioned findings.

These observations further highlight the distinct composition of EVP proteomes that result from different isolation procedures. The improved EVP purity enables the detection of low abundance proteins and helps identify potential contaminants present in plasma EVPs.

3.6 | Identification of potential contaminants and novel protein cargos in plasma EVPs isolated using UC-based approaches

Since UC3 and UC2-qEV effectively enhance the purity of plasma EVPs, we further analyzed the proteins that were specifically enriched or depleted in these samples compared to UC2. This allowed us to define common contaminants in plasma EVPs and potential novel EVP cargos uncovered using these protocols. To accomplish this, we utilized the criteria of log2 fold change (FC) > 1.5 and adjusted p value (padj) < 0.05 to identify the differentially detected proteins (DDPs) between UC2 samples and samples prepared using other protocols. As shown in the Venn diagrams (Figure 3a) and consistent with the aforementioned PCA results, we found that UC3 and UC2-qEV samples had a higher degree of similarity to each other, with a greater overlap of DDPs in both enriched and depleted proteins, as compared to UC2. On the other hand, the DDPs identified between PS and UC2 had a minimal overlap with those identified by UC3 and UC2-qEV. Notably, UC2-qEV exhibited the largest number of DDPs among all comparisons, consistent with the highest purity observed for UC2-qEV in our other assays.

Considering the similarity between UC3 and UC2-qEV, we combined the DDPs identified in both protocols versus UC2 for further analysis (see protein lists in Tables 1 and 2). Pathway analysis revealed that DDPs with higher abundance in UC2 products (i.e., potential contaminants in plasma EVPs and depleted by UC3 or UC2-qEV) were associated with complement system and coagulation cascades (Figure 3b). In contrast, DDPs with lower abundance in UC2 products (i.e., enriched by UC3 or UC2-qEV and potential EVP cargos undetected previously in plasma EVPs) were associated with many vesicle regulation-related pathways (Figure 3c). Remarkably, many proteins, including Rab family proteins, transmembrane proteins, and ESCRT members, which are frequently reported as cargo of EVPs isolated from cell culture (e.g., Vesiclepedia, EVpedia, ExoCarta) (Kalra et al., 2012; Kim et al., 2015; Mathivanan & Simpson, 2009), were found among the DDPs enriched by UC3 or UC2-qEV (see Table 2). We also noted that the DDPs with higher abundance in UC2 samples had an overall higher rank of abundance in plasma (range: 1–1127; median: 71; human protein atlas) than those with higher abundance in UC3 and UC2-qEV samples (range: 99–3978; median: 1338) (Figure S7).

TABLE 1 List of proteins enriched by UC2 in comparison to UC3 or UC2-qEV.

Symbol	Entrez gene name	Symbol	Entrez gene name
A1BG	alpha-1-B glycoprotein	FGG	fibrinogen gamma chain
A2M	alpha-2-macroglobulin	FN1	fibronectin 1
AFM	Afamin	GC	GC vitamin D binding protein
AHSG	alpha 2-HS glycoprotein	GPX3	glutathione peroxidase 3
AMBP	alpha-1-microglobulin/bikunin precursor	H2BC12	H2B clustered histone 12
ANG	angiogenin	HABP2	hyaluronan binding protein 2
ANGPTL6	angiopoietin like 6	HPX	hemopexin
APCS	amyloid P component, serum	HRG	histidine rich glycoprotein
APOA4	apolipoprotein A4	IGHG1	immunoglobulin heavy constant gamma 1 (G1m marker)
APOD	apolipoprotein D	IGHG2	immunoglobulin heavy constant gamma 2 (G2m marker)
ATXN1	ataxin 1	IGHG3	immunoglobulin heavy constant gamma 3 (G3m marker)
BANF1	BAF nuclear assembly factor 1	IGHG4	immunoglobulin heavy constant gamma 4 (G4m marker)
C1QA	complement C1q A chain	IGHV3OR16-13	immunoglobulin heavy variable 3/OR16-13 (non-functional)
C1QB	complement C1q B chain	IGKV1-27	immunoglobulin kappa variable 1-27
C1QC	complement C1q C chain	IGKV3-7	immunoglobulin kappa variable 3-7 (non-functional)
C1R	complement C1r	IGKV3OR2-268	immunoglobulin kappa variable 3/OR2-268 (non-functional)
C1RL	complement C1r subcomponent like	IGKV6-21	immunoglobulin kappa variable 6-21 (non-functional)
C1S	complement C1s	ITIH1	inter-alpha-trypsin inhibitor heavy chain 1
C2	complement C2	ITIH2	inter-alpha-trypsin inhibitor heavy chain 2
C3	complement C3	KNG1	kininogen 1
C4A/C4B	complement C4A (Rodgers blood group)	LPA	lipoprotein(a)
C4BPA	complement component 4 binding protein alpha	LRG1	leucine rich alpha-2-glycoprotein 1
C4BPB	complement component 4 binding protein beta	LYZ	lysozyme
C5	complement C5	MASP1	MBL associated serine protease 1
C6	complement C6	NGEF	neuronal guanine nucleotide exchange factor
C7	complement C7	PGLYRP2	peptidoglycan recognition protein 2
C8A	complement C8 alpha chain	PLG	plasminogen
C8B	complement C8 beta chain	PON1	paraoxonase 1
C8G	complement C8 gamma chain	PRG4	proteoglycan 4
C9	complement C9	PROS1	protein S
CFH	complement factor H	PZP	PZP alpha-2-macroglobulin like
CFHR1	complement factor H related 1	RBP4	retinol binding protein 4
CFHR3	complement factor H related 3	RELN	reelin
CFI	complement factor I	RNASE4	ribonuclease A family member 4
CP	ceruloplasmin	SERPINA3	serpin family A member 3
CPN1	carboxypeptidase N subunit 1	SERPINA4	serpin family A member 4
CPN2	carboxypeptidase N subunit 2	SERPINA7	serpin family A member 7
ECM1	extracellular matrix protein 1	SERPINC1	serpin family C member 1
F12	coagulation factor XII	SERPIND1	serpin family D member 1
F13B	coagulation factor XIII B chain	SERPINF2	serpin family F member 2

(Continues)

TABLE 1 (Continued)

Symbol	Entrez gene name	Symbol	Entrez gene name
F2	coagulation factor II, thrombin	SVEP1	sushi, von Willebrand factor type A, EGF and pentraxin domain containing 1
FBLN1	fibulin 1	TTR	transthyretin
FGA	fibrinogen alpha chain	VTN	vitronectin
FGB	fibrinogen beta chain		

The subcellular localization analysis of DDPs revealed that the majority of DDPs depleted by UC3 or UC2-qEV were secreted proteins (Figure 3d). In contrast, most DDPs enriched by UC3 or UC2-qEV were localized either at the plasma membrane or within the cytoplasm, consistent with the idea that they could be packaged within EVPs.

Moreover, searching the PaGenBase database for tissue- and time-specific pattern genes (Pan et al., 2013) (http://bioinf.xmu.edu.cn/PaGenBase/) showed that a large portion of the DDPs enriched using UC2 were proteins produced by the liver, which is the main source of secreted plasma proteins (Trefts et al., 2017) (Figure 3e). In contrast, DDPs enriched using UC3 or UC2-qEV contained an increased proportion of house-keeping and immune-related proteins from tissues such as blood, bone marrow, and spleen (Figure 3e). Overall, the use of UC3 and UC2-qEV effectively eliminates many highly abundant secreted proteins in plasma samples and enhances the detection of specific low-abundance EVP-associated proteins.

3.7 | Distinct plasma EVP protein profiles obtained by PS compared to UC-based approaches

As shown in Figure 3(a), the EVP proteome yielded by PS is distinct from UC-based approaches. A comparison was conducted between the proteomes acquired using PS and all three UC-based methods, and DDPs were identified using the same criteria as described above. DDPs enriched by UC-based methods and PS are listed in Tables 3 and 4, respectively (as well as Figure S8). Pathway analysis revealed that UC-based methods preferentially enriched proteins involved in pathways such as neutrophil degranulation, regulation of opsonization, and 20S proteasome (Figure 4a). In addition, several EVP signature proteins previously identified, including Integrin Alpha 5 (ITGA5), Joining Chain of Multimeric IgA and IgM (JCHAIN), and Galectin 3 Binding Protein (LGALS3BP) (Hoshino et al., 2020; Zhang et al., 2018), were consistently enriched using UC-based protocols (Figure S8a).

The pathways associated with DDPs enriched by PS compared to UC-based methods were significantly different, with the top pathways including complement and coagulation cascades and NABA_core_matrisome, which is an ensemble of core ECM proteins such as ECM glycoproteins, collagens, and proteoglycans (Figure 4a), consistent with the results shown earlier (Figure S6b).

Subcellular localization analysis revealed that a much larger proportion of DDPs enriched using PS were secreted proteins, while DDPs enriched using the UC-based methods consisted of larger proportions of cytoplasmic, nuclear, and plasma membrane-associated proteins (Figure 4b). Furthermore, tissue- and cell type-origin analysis indicated that PS further enriched liver-derived, extracellular proteins (Figure 4c).

Therefore, the heterogeneity of EVPs and the different principles for EVP isolation result in the production of distinct EVP subsets and contaminants when using PS versus UC-based methods. These observations highlight the need for future studies to perform single EVP analysis for further classification of the heterogeneous EVPs and identification of contaminants.

3.8 | Confirming the superior performance of UC3 in isolating EVPs from the plasma of patients with pancreatic cancer

After establishing that UC3 and UC2-qEV approaches yield EVPs with higher purity than UC2 or PS, we proceeded to validate the performance of these optimized methods in human cancer patient samples. Although UC3 and UC2-qEV showed comparable purity and proteome profiles, UC2-qEV requires a larger volume of plasma than UC3, which can be a limitation when using patient samples collected retrospectively. Therefore, we limited our comparison to UC3 and UC2 for cancer patient specimens.

Plasma samples were collected from five early-stage pancreatic cancer (PC) patients and five HDs (see Table S1). These blood samples were collected at the time of surgery from patients who were recently diagnosed with pancreatic cancers. These patients had not received any prior treatment and had no previous cancer diagnoses. Additionally, no metastasis was detected in these patients. The samples were collected in EDTA-tubes and processed using UC2 and UC3 in parallel. In both HD and PC samples, we observed EVPs with higher purity, despite lower protein yield, using UC3 compared to UC2 (Figure S9a, b). Importantly,

TABLE 2 List of proteins enriched by UC3 or UC2-qEV in comparison to UC2.

Symbol	Entrez gene name	Symbol	Entrez gene name
ABCB6	ATP binding cassette subfamily B member 6 (Langereis blood group)	KIF5B	kinesin family member 5B
ABCC1	ATP binding cassette subfamily C member 1	KLC1	kinesin light chain 1
ABCC4	ATP binding cassette subfamily C member 4	KPNB1	karyopherin subunit beta 1
ABCC5	ATP binding cassette subfamily C member 5	KRAS	KRAS proto-oncogene, GTPase
ACTB	actin beta	LAMP2	lysosomal associated membrane protein 2
ACTBL2	actin beta like 2	LAMTOR1	late endosomal/lysosomal adaptor, MAPK and MTOR activator 1
ACTC1	actin alpha cardiac muscle 1	LAMTOR5	late endosomal/lysosomal adaptor, MAPK and MTOR activator 5
ACTR1A	actin related protein 1A	LAP3	leucine aminopeptidase 3
ACTR2	actin related protein 2	LASP1	LIM and SH3 protein 1
ACVR1	activin A receptor type 1	LCN1	lipocalin 1
ADAM17	ADAM metallopeptidase domain 17	LCN2	lipocalin 2
ADH5	alcohol dehydrogenase 5 (class III), chi polypeptide	LCP1	lymphocyte cytosolic protein 1
AGO2	argonaute RISC catalytic component 2	LGALS3	galectin 3
AHCY	adenosylhomocysteinase	LHFPL2	LHFPL tetraspan subfamily member 2
AHNAK	AHNAK nucleoprotein	LMBRD2	LMBR1 domain containing 2
AHSP	alpha hemoglobin stabilizing protein	LNPEP	leucyl and cystinyl aminopeptidase
AK1	adenylate kinase 1	LRRC8D	leucine rich repeat containing 8 VRAC subunit D
ALOX12	arachidonate 12-lipoxygenase, 12S type	LRSAM1	leucine rich repeat and sterile alpha motif containing 1
ALPL	alkaline phosphatase, biomineralization associated	LSM4	LSM4 homolog, U6 small nuclear RNA and mRNA degradation associated
AMPD2	adenosine monophosphate deaminase 2	MARCHF8	membrane associated ring-CH-type finger 8
ANK1	ankyrin 1	MARCKSL1	MARCKS like 1
ANPEP	alanyl aminopeptidase, membrane	MBP	myelin basic protein
ANXA1	annexin A1	MDH1	malate dehydrogenase 1
ANXA11	annexin A11	MDH2	malate dehydrogenase 2
ANXA2	annexin A2	MFGE8	milk fat globule EGF and factor V/VIII domain containing
ANXA4	annexin A4	MGLL	monoglyceride lipase
ANXA6	annexin A6	MINK1	misshapen like kinase 1
AP1B1	adaptor related protein complex 1 subunit beta 1	MME	membrane metalloendopeptidase
AP1G1	adaptor related protein complex 1 subunit gamma 1	MPP1	MAGUK p55 scaffold protein 1
AP1M1	adaptor related protein complex 1 subunit mu 1	MSN	Moesin
AP2M1	adaptor related protein complex 2 subunit mu 1	MVP	major vault protein
APRT	adenine phosphoribosyltransferase	MYO1G	myosin IG
AQP1	aquaporin 1 (Colton blood group)	NAP1L4	nucleosome assembly protein 1 like 4
ARF6	ADP ribosylation factor 6	NAPG	NSF attachment protein gamma
ARHGAP1	Rho GTPase activating protein 1	NCKAP1	NCK associated protein 1
ARHGAP17	Rho GTPase activating protein 17	NCKAP1L	NCK associated protein 1 like
ARHGAP18	Rho GTPase activating protein 18	NECTIN2	nectin cell adhesion molecule 2

(Continues)

TABLE 2 (Continued)

Symbol	Entrez gene name	Symbol	Entrez gene name
ARPC2	actin related protein 2/3 complex subunit 2	NME1-NME2	NME1-NME2 readthrough
ARPC5	actin related protein 2/3 complex subunit 5	NPEPPS	aminopeptidase puromycin sensitive
ATIC	5-aminoimidazole-4-carboxamide ribonucleotide formyltransferase/IMP cyclohydrolase	NPTN	neuroplastin
ATP11B	ATPase phospholipid transporting 11B (putative)	NRAS	NRAS proto-oncogene, GTPase
ATP1A1	ATPase Na+/K+ transporting subunit alpha 1	NRGN	neurogranin
ATP1B3	ATPase Na+/K+ transporting subunit beta 3	NSF	N-ethylmaleimide sensitive factor, vesicle fusing ATPase
ATP5F1A	ATP synthase F1 subunit alpha	NT5E	5′-nucleotidase ecto
ATP5F1B	ATP synthase F1 subunit beta	NUTF2	nuclear transport factor 2
ATP6AP1	ATPase H+ transporting accessory protein 1	OLFM4	olfactomedin 4
ATP6V0A2	ATPase H+ transporting V0 subunit a2	OXSR1	oxidative stress responsive kinase 1
ATP6V1A	ATPase H+ transporting V1 subunit A	P2RY12	purinergic receptor P2Y12
ATP6V1B2	ATPase H+ transporting V1 subunit B2	PACSIN2	protein kinase C and casein kinase substrate in neurons 2
ATP6V1E1	ATPase H+ transporting V1 subunit E1	PAICS	phosphoribosylaminoimidazole carboxylase and phosphoribosylaminoimidazolesuccinocarboxamide synthase
ATP6V1G1	ATPase H+ transporting V1 subunit G1	PARK7	Parkinsonism associated deglycase
ATP6V1H	ATPase H+ transporting V1 subunit H	PDCD6	programmed cell death 6
ATP7A	ATPase copper transporting alpha	PDCD6IP	programmed cell death 6 interacting protein
BAG2	BAG cochaperone 2	PDE5A	phosphodiesterase 5A
BAIAP2	BAR/IMD domain containing adaptor protein 2	PDIA6	protein disulfide isomerase family A member 6
BCAM	basal cell adhesion molecule (Lutheran blood group)	PDLIM1	PDZ and LIM domain 1
BLMH	bleomycin hydrolase	PEA15	proliferation and apoptosis adaptor protein 15
BLVRA	biliverdin reductase A	PEBP1	phosphatidylethanolamine binding protein 1
BLVRB	biliverdin reductase B	PFKP	phosphofructokinase, platelet
BROX	BRO1 domain and CAAX motif containing	PGAM1	phosphoglycerate mutase 1
BTK	Bruton tyrosine kinase	PGD	phosphogluconate dehydrogenase
C2orf88	chromosome 2 open reading frame 88	PGK1	phosphoglycerate kinase 1
CA1	carbonic anhydrase 1	PGRMC1	progesterone receptor membrane component 1
CA2	carbonic anhydrase 2	PI4K2A	phosphatidylinositol 4-kinase type 2 alpha
CALM1 (includes others)	calmodulin 1	PIP	prolactin induced protein
CALR	calreticulin	PIP4K2A	phosphatidylinositol-5-phosphate 4-kinase type 2 alpha
CAND1	cullin associated and neddylation dissociated 1	PKM	pyruvate kinase M1/2
CANX	calnexin	PLS3	plastin 3
CAPN5	calpain 5	PLSCR1	phospholipid scramblase 1
CCL5	C-C motif chemokine ligand 5	PLXNA4	plexin A4
CCRL2	C-C motif chemokine receptor like 2	PLXNB2	plexin B2
CCT5	chaperonin containing TCP1 subunit 5	PLXNB3	plexin B3
CCT7	chaperonin containing TCP1 subunit 7	PNP	purine nucleoside phosphorylase

(Continues)

TABLE 2 (Continued)

Symbol	Entrez gene name	Symbol	Entrez gene name
CD109	CD109 molecule	PODXL	podocalyxin like
CD2	CD2 molecule	PPBP	pro-platelet basic protein
CD2AP	CD2 associated protein	PPIA	peptidylprolyl isomerase A
Symbol	**Entrez Gene Name**	**Symbol**	**Entrez Gene Name**
CD3E	CD3 epsilon subunit of T-cell receptor complex	PPIB	peptidylprolyl isomerase B
CD44	CD44 molecule (Indian blood group)	PPIF	peptidylprolyl isomerase F
CD46	CD46 molecule	PPM1A	protein phosphatase, Mg2+/Mn2+ dependent 1A
CD47	CD47 molecule	PPP1R21	protein phosphatase 1 regulatory subunit 21
CD48	CD48 molecule	PRDX5	peroxiredoxin 5
CD5	CD5 molecule	PRKACA	protein kinase cAMP-activated catalytic subunit alpha
CD55	CD55 molecule (Cromer blood group)	PRKACB	protein kinase cAMP-activated catalytic subunit beta
CD58	CD58 molecule	PRPS1	phosphoribosyl pyrophosphate synthetase 1
CD6	CD6 molecule	PSMB1	proteasome 20S subunit beta 1
CD69	CD69 molecule	PSMB10	proteasome 20S subunit beta 10
CD81	CD81 molecule	PSMB3	proteasome 20S subunit beta 3
CD82	CD82 molecule	PSME1	proteasome activator subunit 1
CD84	CD84 molecule	PSTPIP2	proline-serine-threonine phosphatase interacting protein 2
CD9	CD9 molecule	PTGES3	prostaglandin E synthase 3
CDC37	cell division cycle 37, HSP90 cochaperone	PTGS1	prostaglandin-endoperoxide synthase 1
CDC42	cell division cycle 42	PTMA	prothymosin alpha
CFL1	cofilin 1	PTP4A2	protein tyrosine phosphatase 4A2
CHMP2A	charged multivesicular body protein 2A	PTPN23	protein tyrosine phosphatase non-receptor type 23
CHMP2B	charged multivesicular body protein 2B	PTPRA	protein tyrosine phosphatase receptor type A
CHMP4A	charged multivesicular body protein 4A	RAB11B	RAB11B, member RAS oncogene family
CHMP4B	charged multivesicular body protein 4B	RAB14	RAB14, member RAS oncogene family
CHMP5	charged multivesicular body protein 5	RAB21	RAB21, member RAS oncogene family
CIB1	calcium and integrin binding 1	RAB2A	RAB2A, member RAS oncogene family
CLC	Charcot-Leyden crystal galectin	RAB2B	RAB2B, member RAS oncogene family
CLEC1B	C-type lectin domain family 1 member B	RAB35	RAB35, member RAS oncogene family
CLEC4M	C-type lectin domain family 4 member M	RAB7A	RAB7A, member RAS oncogene family
CLIC1	chloride intracellular channel 1	RAB8A	RAB8A, member RAS oncogene family
CLIC2	chloride intracellular channel 2	RAB8B	RAB8B, member RAS oncogene family
CLIC4	chloride intracellular channel 4	RABEP1	rabaptin, RAB GTPase binding effector protein 1
CLINT1	clathrin interactor 1	RAC1	Rac family small GTPase 1
CMIP	c-Maf inducing protein	RAC2	Rac family small GTPase 2
CNDP2	carnosine dipeptidase 2	RALB	RAS like proto-oncogene B
CNNM2	cyclin and CBS domain divalent metal cation transport mediator 2	RAN	RAN, member RAS oncogene family
CNNM4	cyclin and CBS domain divalent metal cation transport mediator 4	RAP1A	RAP1A, member of RAS oncogene family
CNP	2′,3′-cyclic nucleotide 3′ phosphodiesterase	RAP1B	RAP1B, member of RAS oncogene family
COL6A3	collagen type VI alpha 3 chain	RAP2B	RAP2B, member of RAS oncogene family
CORO1B	coronin 1B	RAP2C	RAP2C, member of RAS oncogene family
COTL1	coactosin like F-actin binding protein 1	RASGRP2	RAS guanyl releasing protein 2

(Continues)

TABLE 2 (Continued)

Symbol	Entrez gene name	Symbol	Entrez gene name
CPNE1	copine 1	RDX	radixin
CRIP1	cysteine rich protein 1	REEP5	receptor accessory protein 5
CRIP2	cysteine rich protein 2	RFFL	ring finger and FYVE like domain containing E3 ubiquitin protein ligase
CRKL	CRK like proto-oncogene, adaptor protein	RFTN1	raftlin, lipid raft linker 1
CRYZL1	crystallin zeta like 1	RGS18	regulator of G protein signaling 18
CS	citrate synthase	RHAG	Rh associated glycoprotein
CSK	C-terminal Src kinase	RHCE/RHD	Rh blood group D antigen
CTSA	cathepsin A	RHOA	ras homolog family member A
CYBRD1	cytochrome b reductase 1	RHOF	ras homolog family member F, filopodia associated
CYC1	cytochrome c1	ROCK2	Rho associated coiled-coil containing protein kinase 2
CYCS	cytochrome c, somatic	S100A10	S100 calcium binding protein A10
CYRIB	CYFIP related Rac1 interactor B	S100A11	S100 calcium binding protein A11
DAAM1	dishevelled associated activator of morphogenesis 1	S100A7	S100 calcium binding protein A7
DBI	diazepam binding inhibitor, acyl-CoA binding protein	S100A9	S100 calcium binding protein A9
DBNL	drebrin like	SCAMP2	secretory carrier membrane protein 2
DCD	dermcidin	SDCBP	syndecan binding protein
DDAH2	dimethylarginine dimethylaminohydrolase 2	SEC24C	SEC24 homolog C, COPII coat complex component
DDT	D-dopachrome tautomerase	SELL	selectin L
DERA	deoxyribose-phosphate aldolase	SELP	selectin P
DNAJA2	DnaJ heat shock protein family (Hsp40) member A2	SEMA7A	semaphorin 7A (John Milton Hagen blood group)
DNAJA4	DnaJ heat shock protein family (Hsp40) member A4	SEPTIN11	septin 11
DNAJB1	DnaJ heat shock protein family (Hsp40) member B1	SEPTIN6	septin 6
DNAJB4	DnaJ heat shock protein family (Hsp40) member B4	SERINC3	serine incorporator 3
DNAJC5	DnaJ heat shock protein family (Hsp40) member C5	SERPINB9	serpin family B member 9
DNAJC7	DnaJ heat shock protein family (Hsp40) member C7	SKP1	S-phase kinase associated protein 1
DNM1	dynamin 1	SLC11A2	solute carrier family 11 member 2
DOCK10	dedicator of cytokinesis 10	SLC12A4	solute carrier family 12 member 4
DPP4	dipeptidyl peptidase 4	SLC12A6	solute carrier family 12 member 6
DPYSL2	dihydropyrimidinase like 2	SLC12A7	solute carrier family 12 member 7
DYNLL2	dynein light chain LC8-type 2	SLC16A1	solute carrier family 16 member 1
ECE1	endothelin converting enzyme 1	SLC16A7	solute carrier family 16 member 7
EFR3A	EFR3 homolog A	SLC1A4	solute carrier family 1 member 4
EHD1	EH domain containing 1	SLC1A5	solute carrier family 1 member 5
EIF5A	eukaryotic translation initiation factor 5A	SLC22A16	solute carrier family 22 member 16
ELOC	elongin C	SLC25A3	solute carrier family 25 member 3
EMCN	endomucin	SLC25A5	solute carrier family 25 member 5
EMILIN1	elastin microfibril interfacer 1	SLC29A1	solute carrier family 29 member 1 (Augustine blood group)

(Continues)

TABLE 2 (Continued)

Symbol	Entrez gene name	Symbol	Entrez gene name
ENDOD1	endonuclease domain containing 1	SLC2A1	solute carrier family 2 member 1
ENO1	enolase 1	SLC3A2	solute carrier family 3 member 2
ENO2	enolase 2	SLC40A1	solute carrier family 40 member 1
ENPEP	glutamyl aminopeptidase	SLC43A1	solute carrier family 43 member 1
Symbol	**Entrez Gene Name**	**Symbol**	**Entrez Gene Name**
EPB41	erythrocyte membrane protein band 4.1	SLC43A3	solute carrier family 43 member 3
ERBIN	erbb2 interacting protein	SLC44A2	solute carrier family 44 member 2
ESD	esterase D	SLC4A1	solute carrier family 4 member 1 (Diego blood group)
EZR	ezrin	SLC7A1	solute carrier family 7 member 1
F2R	coagulation factor II thrombin receptor	SLC7A5	solute carrier family 7 member 5
FABP4	fatty acid binding protein 4	SLC9A3R1	SLC9A3 regulator 1
FABP5	fatty acid binding protein 5	SLC9A3R2	SLC9A3 regulator 2
FAM151A	family with sequence similarity 151 member A	SNTB1	syntrophin beta 1
FAM234B	family with sequence similarity 234 member B	SNX12	sorting nexin 12
FAS	Fas cell surface death receptor	SNX3	sorting nexin 3
FBN1	fibrillin 1	SOD1	superoxide dismutase 1
FCGR2A	Fc gamma receptor IIa	SOD2	superoxide dismutase 2
FCGRT	Fc gamma receptor and transporter	SRGN	serglycin
FDPS	farnesyl diphosphate synthase	ST13	ST13 Hsp70 interacting protein
FHL1	four and a half LIM domains 1	STAM	signal transducing adaptor molecule
FIS1	fission, mitochondrial 1	STAM2	signal transducing adaptor molecule 2
FKBP1A	FKBP prolyl isomerase 1A	STAT5A	signal transducer and activator of transcription 5A
FLII	FLII actin remodeling protein	STEAP3	STEAP3 metalloreductase
FLOT2	flotillin 2	STIM1	stromal interaction molecule 1
FYB1	FYN binding protein 1	STIP1	stress induced phosphoprotein 1
GABARAPL2	GABA type A receptor associated protein like 2	STK10	serine/threonine kinase 10
GAPDH	glyceraldehyde-3-phosphate dehydrogenase	STK24	serine/threonine kinase 24
GCA	grancalcin	STK26	serine/threonine kinase 26
GDI1	GDP dissociation inhibitor 1	STX12	syntaxin 12
GDI2	GDP dissociation inhibitor 2	STX16	syntaxin 16
GGT1	gamma-glutamyltransferase 1	STX4	syntaxin 4
GLIPR2	GLI pathogenesis related 2	STX6	syntaxin 6
GMPR	guanosine monophosphate reductase	STX8	syntaxin 8
GNA13	G protein subunit alpha 13	SUSD3	sushi domain containing 3
GNAI1	G protein subunit alpha i1	SYNGR2	synaptogyrin 2
GNAI2	G protein subunit alpha i2	SYTL4	synaptotagmin like 4
GNAI3	G protein subunit alpha i3	TALDO1	transaldolase 1
GNB1	G protein subunit beta 1	TBXAS1	thromboxane A synthase 1
GNG10	G protein subunit gamma 10	TCP1	t-complex 1
GNG11	G protein subunit gamma 11	TESC	tescalcin
GNG2	G protein subunit gamma 2	TFRC	transferrin receptor
GNG5	G protein subunit gamma 5	TGFBRAP1	transforming growth factor beta receptor associated protein 1

(Continues)

TABLE 2 (Continued)

Symbol	Entrez gene name	Symbol	Entrez gene name
GNG7	G protein subunit gamma 7	TKT	transketolase
GOLGA7	golgin A7	TM4SF4	transmembrane 4 L six family member 4
GPI	glucose-6-phosphate isomerase	TM9SF2	transmembrane 9 superfamily member 2
GPRC5C	G protein-coupled receptor class C group 5 member C	TMEM9B	TMEM9 domain family member B
GPX1	glutathione peroxidase 1	TNIK	TRAF2 and NCK interacting kinase
GPX4	glutathione peroxidase 4	TPM3	tropomyosin 3
GRK6	G protein-coupled receptor kinase 6	TPM4	tropomyosin 4
GSR	glutathione-disulfide reductase	TRBC1	T cell receptor beta constant 1
GSTM5	glutathione S-transferase mu 5	TRPC6	transient receptor potential cation channel subfamily C member 6
GSTO1	glutathione S-transferase omega 1	TSG101	tumor susceptibility 101
GSTP1	glutathione S-transferase pi 1	TSPAN14	tetraspanin 14
GTPBP2	GTP binding protein 2	TSPAN32	tetraspanin 32
GYPC	glycophorin C (Gerbich blood group)	TSPAN4	tetraspanin 4
HBA1/HBA2	hemoglobin subunit alpha 2	TWF2	twinfilin actin binding protein 2
HBB	hemoglobin subunit beta	TXN	thioredoxin
HBD	hemoglobin subunit delta	TXNL1	thioredoxin like 1
HEBP2	heme binding protein 2	UBA7	ubiquitin like modifier activating enzyme 7
HPRT1	hypoxanthine phosphoribosyltransferase 1	UBASH3B	ubiquitin associated and SH3 domain containing B
HPSE	heparanase	UBC	ubiquitin C
HSD17B4	hydroxysteroid 17-beta dehydrogenase 4	UBE2L3	ubiquitin conjugating enzyme E2 L3
HSP90AB1	heat shock protein 90 alpha family class B member 1	UBE2V1	ubiquitin conjugating enzyme E2 V1
HSP90B1	heat shock protein 90 beta family member 1	UMAD1	UBAP1-MVB12-associated (UMA) domain containing 1
HSPA2	heat shock protein family A (Hsp70) member 2	USP8	ubiquitin specific peptidase 8
HSPA4	heat shock protein family A (Hsp70) member 4	VAMP3	vesicle associated membrane protein 3
HSPA6	heat shock protein family A (Hsp70) member 6	VAMP5	vesicle associated membrane protein 5
HSPA8	heat shock protein family A (Hsp70) member 8	VAMP7	vesicle associated membrane protein 7
HSPD1	heat shock protein family D (Hsp60) member 1	VAMP8	vesicle associated membrane protein 8
HSPE1	heat shock protein family E (Hsp10) member 1	VNN1	vanin 1
ICAM1	intercellular adhesion molecule 1	VPS11	VPS11 core subunit of CORVET and HOPS complexes
ICAM3	intercellular adhesion molecule 3	VPS28	VPS28 subunit of ESCRT-I
IDH1	isocitrate dehydrogenase (NADP(+)) 1	VPS35	VPS35 retromer complex component
IGSF8	immunoglobulin superfamily member 8	VPS37B	VPS37B subunit of ESCRT-I
IPO5	importin 5	VPS4A	vacuolar protein sorting 4 homolog A
IQGAP1	IQ motif containing GTPase activating protein 1	VPS4B	vacuolar protein sorting 4 homolog B

(Continues)

TABLE 2 (Continued)

Symbol	Entrez gene name	Symbol	Entrez gene name
IQGAP2	IQ motif containing GTPase activating protein 2	VPS8	VPS8 subunit of CORVET complex
IST1	IST1 factor associated with ESCRT-III	VTA1	vesicle trafficking 1
ITGA4	integrin subunit alpha 4	VTI1B	vesicle transport through interaction with t-SNAREs 1B
ITGA6	integrin subunit alpha 6	WARS1	tryptophanyl-tRNA synthetase 1
ITGAL	integrin subunit alpha L	WASF2	WASP family member 2
ITGAM	integrin subunit alpha M	WASF3	WASP family member 3
ITGB1	integrin subunit beta 1	WBP2	WW domain binding protein 2
ITGB2	integrin subunit beta 2	WDSUB1	WD repeat, sterile alpha motif and U-box domain containing 1
KALRN	kalirin RhoGEF kinase	XPO1	exportin 1
KATNAL2	katanin catalytic subunit A1 like 2	YKT6	YKT6 v-SNARE homolog
KEL	Kell metallo-endopeptidase (Kell blood group)	YWHAE	tyrosine 3-monooxygenase/tryptophan 5-monooxygenase activation protein epsilon
KIF2A	kinesin family member 2A	ZDHHC2	zinc finger DHHC-type palmitoyltransferase 2

proteomic MS revealed a 25%–30% increase in the total number of proteins identified in EVPs isolated using UC3 compared to UC2 in both PC and HD samples (Figure S9c).

Proteomics analysis further confirmed the enrichment of conventional EVP markers (Figure S9d) and signature proteins associated with exosomes (Figure S9e) in EVPs isolated by UC3 from both HD and PC groups. Furthermore, GSEA confirmed the depletion of contaminating plasma proteins when using UC3 compared to UC2 (Figure S9f). As expected, we also observed enrichment of ITG family members and depletion of apolipoproteins using UC3 in both PC and HD specimens (Figure S9g, h). Due to the small number of exomere-associated signature proteins detected in these samples, we could not perform GSEA to evaluate whether they were further enriched by UC3.

Differentially expressed proteins (DEPs) in EVPs isolated from PC and HD plasma have the potential to serve as biomarker candidates to distinguish cancer patients from healthy controls and enabling early detection. To identify such candidates, we applied stringent criteria of >5-fold difference in abundance and at least 40% detection frequency (i.e., detected in at least two out of five samples per group). Importantly, 14% of total proteins (58 DEPs out of an average of 422 total proteins, Table S2) were found to be differentially expressed between PC and HD EVPs isolated through UC3, which was much higher than the 9% (29 DEPs out of an average of 327 total proteins, Table S3) identified between PC and HD EVPs isolated through UC2 (Figure S9i). These findings strongly support that by improving EVP quality with UC3, a more in-depth analysis of plasma-derived EVP proteomes can expand the pool of candidates for biomarker discovery. While the inclusion of this small set of patient samples further confirms the improvements in EVP purity and protein detection achieved through our optimized methods, we must acknowledge that this sample size is inadequate for the identification and validation of cancer-specific biomarkers due to the inherent variability among individual patient samples and the presence of numerous confounding factors within these samples. Although beyond the scope of this study, larger patient cohorts should be examined in the future to rigorously test this hypothesis.

4 | DISCUSSION

In this study, we compared different methods for isolating circulating EVPs from plasma, including modified UC-based approaches, the phosphatidylserine-Tim 4 interaction-based affinity capturing kit, and several other commercial kits. Our results showed that the modified UC-based approaches, namely, UC3 and UC2-qEV, yielded EVPs with significantly improved purity compared to the commonly used UC2 method. This was demonstrated by increased levels of conventional EVP markers, systemic enrichment of exosome- and exomere-associated signatures, and identification of a large number of low-abundance proteins. Importantly, many of the newly identified or further enriched proteins were plasma membrane-bound or cytoplasmic proteins and functionally associated with vesicle-related pathways, supporting their identity as bona fide plasma EVP cargo. Future studies using single EVP analysis could further validate and confirm these newly identified proteins as plasma EVP cargo. Significantly, using UC3, we identified a larger set of DEPs between cancer patients and healthy controls, which provides opportunities for potential biomarker discovery. Future studies with larger cohorts of cancer patients and controls will be needed to further validate the utility of UC3 for identifying potential diagnostic and prognostic biomarkers.

TABLE 3 List of proteins enriched by UC-based methods in comparison to PS.

Symbol	Entrez Gene Name	Symbol	Entrez Gene Name
A2M	alpha-2-macroglobulin	JCHAIN	joining chain of multimeric IgA and IgM
ACTR1A	actin related protein 1A	KALRN	kalirin RhoGEF kinase
ADIPOQ	adiponectin, C1Q and collagen domain containing	KCTD12	potassium channel tetramerization domain containing 12
AHCY	adenosylhomocysteinase	LAMP2	lysosomal associated membrane protein 2
AHNAK	AHNAK nucleoprotein	LAMTOR5	late endosomal/lysosomal adaptor, MAPK and MTOR activator 5
ALDH16A1	aldehyde dehydrogenase 16 family member A1	LAP3	leucine aminopeptidase 3
ANGPTL3	angiopoietin like 3	LCN2	lipocalin 2
ANPEP	alanyl aminopeptidase, membrane	LECT2	leukocyte cell derived chemotaxin 2
AP2M1	adaptor related protein complex 2 subunit mu 1	LGALS3BP	galectin 3 binding protein
APOL1	apolipoprotein L1	MASP2	MBL associated serine protease 2
ARHGDIA	Rho GDP dissociation inhibitor alpha	MGLL	monoglyceride lipase
ATP1B3	ATPase Na+/K+ transporting subunit beta 3	MME	membrane metalloendopeptidase
ATP6V1B2	ATPase H+ transporting V1 subunit B2	MVP	major vault protein
ATP6V1G1	ATPase H+ transporting V1 subunit G1	MYH1	myosin heavy chain 1
BAIAP2	BAR/IMD domain containing adaptor protein 2	MYH2	myosin heavy chain 2
BANF1	BAF nuclear assembly factor 1	MYH4	myosin heavy chain 4
C1QTNF3	C1q and TNF related 3	MYH7	myosin heavy chain 7
C4BPA	complement component 4 binding protein alpha	MYH7B	myosin heavy chain 7B
C4BPB	complement component 4 binding protein beta	MYO1C	myosin IC
CALHM5	calcium homeostasis modulator family member 5	MYO1G	myosin IG
CCT2	chaperonin containing TCP1 subunit 2	NPTN	neuroplastin
CCT5	chaperonin containing TCP1 subunit 5	NRAS	NRAS proto-oncogene, GTPase
CD46	CD46 molecule	NT5E	5′-nucleotidase ecto
CD48	CD48 molecule	OLFM4	olfactomedin 4
CD5L	CD5 molecule like	OSTF1	osteoclast stimulating factor 1
CD69	CD69 molecule	PAICS	phosphoribosylaminoimidazole carboxylase and phosphoribosylaminoimidazolesuccinocarboxamide synthase
CHMP4B	charged multivesicular body protein 4B	PANX1	pannexin 1
CHMP5	charged multivesicular body protein 5	PEBP1	phosphatidylethanolamine binding protein 1
CLIC2	chloride intracellular channel 2	PIGR	polymeric immunoglobulin receptor
CLIC4	chloride intracellular channel 4	PLXNB2	plexin B2
CLINT1	clathrin interactor 1	PODXL	podocalyxin like
COLEC10	collectin subfamily member 10	PRKCD	protein kinase C delta
COLEC11	collectin subfamily member 11	PRKCQ	protein kinase C theta
CRIP2	cysteine rich protein 2	PSMA2	proteasome 20S subunit alpha 2
CRKL	CRK like proto-oncogene, adaptor protein	PSMA3	proteasome 20S subunit alpha 3
CRYZL1	crystallin zeta like 1	PSMA4	proteasome 20S subunit alpha 4
CTTN	cortactin	PSMA6	proteasome 20S subunit alpha 6
DBI	diazepam binding inhibitor, acyl-CoA binding protein	PSMA7	proteasome 20S subunit alpha 7
DERA	deoxyribose-phosphate aldolase	PSMB1	proteasome 20S subunit beta 1
DNM2	dynamin 2	PSMB3	proteasome 20S subunit beta 3
DPP4	dipeptidyl peptidase 4	PSMB8	proteasome 20S subunit beta 8
ELOC	elongin C	PTP4A2	protein tyrosine phosphatase 4A2
EMCN	endomucin	PZP	PZP alpha-2-macroglobulin like

(Continues)

TABLE 3 (Continued)

Symbol	Entrez Gene Name	Symbol	Entrez Gene Name
ENPP4	ectonucleotide pyrophosphatase/phosphodiesterase 4	RAB2A	RAB2A, member RAS oncogene family
EPS8	epidermal growth factor receptor pathway substrate 8	RAP2C	RAP2C, member of RAS oncogene family
ERN1	endoplasmic reticulum to nucleus signaling 1	RELN	reelin
EXTL2	exostosin like glycosyltransferase 2	RHOF	ras homolog family member F, filopodia associated
FCGBP	Fc gamma binding protein	RP2	RP2 activator of ARL3 GTPase
FCN1	ficolin 1	RRAS	RAS related
FCN2	ficolin 2	S100A10	S100 calcium binding protein A10
FCN3	ficolin 3	S100A12	S100 calcium binding protein A12
FKBP1A	FKBP prolyl isomerase 1A	SERINC3	serine incorporator 3
FMNL1	formin like 1	SERPINB1	serpin family B member 1
FTH1	ferritin heavy chain 1	SLC22A16	solute carrier family 22 member 16
GNG7	G protein subunit gamma 7	SLC7A5	solute carrier family 7 member 5
GPRC5C	G protein-coupled receptor class C group 5 member C	SLC9A3R2	SLC9A3 regulator 2
GPX4	glutathione peroxidase 4	SOD2	superoxide dismutase 2
H4C1	H4 clustered histone 1	SPPL2A	signal peptide peptidase like 2A
HSP90B1	heat shock protein 90 beta family member 1	ST8SIA4	ST8 alpha-N-acetyl-neuraminide alpha-2,8-sialyltransferase 4
IDH1	isocitrate dehydrogenase (NADP(+)) 1	STAM2	signal transducing adaptor molecule 2
IGHM	immunoglobulin heavy constant mu	STAT3	signal transducer and activator of transcription 3
IGHV2-26	immunoglobulin heavy variable 2-26	STAT5A	signal transducer and activator of transcription 5A
IGHV2-5	immunoglobulin heavy variable 2-5	STX6	syntaxin 6
IGHV2-70	immunoglobulin heavy variable 2-70	SVEP1	sushi, von Willebrand factor type A, EGF and pentraxin domain containing 1
IGHV3OR15-7	immunoglobulin heavy variable 3/OR15-7 (pseudogene)	TCP1	t-complex 1
IGHV4-4	immunoglobulin heavy variable 4-4	TGFB1I1	transforming growth factor beta 1 induced transcript 1
IGKV1-16	immunoglobulin kappa variable 1-16	TMOD3	tropomodulin 3
IGLV1-51	immunoglobulin lambda variable 1-51	TPD52L2	TPD52 like 2
IGLV2-11	immunoglobulin lambda variable 2-11	TPP2	tripeptidyl peptidase 2
IGLV2-14	immunoglobulin lambda variable 2-14	TSPAN2	tetraspanin 2
IGLV2-23	immunoglobulin lambda variable 2-23	TTN	titin
IGLV2-8	immunoglobulin lambda variable 2-8	UBA7	ubiquitin like modifier activating enzyme 7
IGLV3-16	immunoglobulin lambda variable 3-16	UMAD1	UBAP1-MVB12-associated (UMA) domain containing 1
IGLV3-27	immunoglobulin lambda variable 3-27	USP8	ubiquitin specific peptidase 8
IGLV4-60	immunoglobulin lambda variable 4-60	VAMP7	vesicle associated membrane protein 7
INPP5A	inositol polyphosphate-5-phosphatase A	VPS37B	VPS37B subunit of ESCRT-I
IQGAP1	IQ motif containing GTPase activating protein 1	WASF3	WASP family member 3
ITGA5	integrin subunit alpha 5		

Specifically, by comparing the optimized UC3 and UC2-qEV with the traditional UC2 approach, we observed significant reduction in contaminants, notably apolipoproteins and top-ranked secreted plasma proteins in the samples isolated through UC3 and UC2-qEV. However, we observed no consistent trend of depletion or enrichment for most immunoglobulins in the plasma EVPs. The configuration of immunoglobulins (i.e., soluble vs. EVP-associated, externally bound to vs. internally packaged into EVPs) for each class and isotype of immunoglobulins is a complex area of research that requires further assessment. Further research is necessary to elucidate the functional regulation of immunoglobulins associated with EVPs and their translational potential as biomarkers under different pathological conditions.

TABLE 4 List of proteins enriched by PS in comparison to UC-based methods.

Symbol	Entrez Gene Name	Symbol	Entrez Gene Name
A1BG	alpha-1-B glycoprotein	GC	GC vitamin D binding protein
ABCB9	ATP binding cassette subfamily B member 9	GPLD1	glycosylphosphatidylinositol specific phospholipase D1
AFM	afamin	GPX3	glutathione peroxidase 3
AMBP	alpha-1-microglobulin/bikunin precursor	HPX	hemopexin
ANXA3	annexin A3	HRNR	hornerin
ANXA4	annexin A4	HSPG2	heparan sulfate proteoglycan 2
ANXA5	annexin A5	IGKV3-7	immunoglobulin kappa variable 3-7 (non-functional)
APCS	amyloid P component, serum	ITLN1	intelectin 1
APOA4	apolipoprotein A4	ITLN2	intelectin 2
BTD	biotinidase	KNG1	kininogen 1
C2	complement C2	KRT13	keratin 13
C8G	complement C8 gamma chain	LAMTOR4	late endosomal/lysosomal adaptor, MAPK and MTOR activator 4
CETP	cholesteryl ester transfer protein	LPA	lipoprotein(a)
CFD	complement factor D	LRG1	leucine rich alpha-2-glycoprotein 1
CFH	complement factor H	LRRC4	leucine rich repeat containing 4
CFHR1	complement factor H related 1	MFAP4	microfibril associated protein 4
CLEC3B	C-type lectin domain family 3 member B	MGP	matrix Gla protein
COL6A1	collagen type VI alpha 1 chain	MST1	macrophage stimulating 1
CP	ceruloplasmin	ORM1	orosomucoid 1
CPN1	carboxypeptidase N subunit 1	PCOLCE	procollagen C-endopeptidase enhancer
CRNN	cornulin	PGLYRP2	peptidoglycan recognition protein 2
CRP	C-reactive protein	PIP	prolactin induced protein
DMTN	dematin actin binding protein	PLG	plasminogen
ECM1	extracellular matrix protein 1	RARRES2	retinoic acid receptor responder 2
EFEMP1	EGF containing fibulin extracellular matrix protein 1	SAA1	serum amyloid A1
EPB41L3	erythrocyte membrane protein band 4.1 like 3	SAA2	serum amyloid A2
F10	coagulation factor X	SERPINA1	serpin family A member 1
F13B	coagulation factor XIII B chain	SERPINA4	serpin family A member 4
F9	coagulation factor IX	SERPINA6	serpin family A member 6
FBLN1	fibulin 1	SERPINA7	serpin family A member 7
FBLN2	fibulin 2	SERPINC1	serpin family C member 1
FBLN5	fibulin 5	SERPINF1	serpin family F member 1
FGA	fibrinogen alpha chain	SERPINF2	serpin family F member 2
FGB	fibrinogen beta chain	SLC43A1	solute carrier family 43 member 1
FGG	fibrinogen gamma chain	TIMD4	T cell immunoglobulin and mucin domain containing 4
FN1	fibronectin 1	TTR	transthyretin

Our analysis revealed a distinct proteome composition of plasma EVPs isolated using the PS approach. Specifically, we observed a biased enrichment for EVP subsets carrying FLOT1 and FLOT2, but not those carrying tetraspanins (such as CD81, CD9 and CD63), Tsg101, or PDCD6IP/Alix. Furthermore, compared to UC2, PS was found to enrich for certain exosome signatures, but not those of exomeres, likely due to the lower level and configuration of phosphatidylserine present in exomeres (Zhang et al., 2018). Notably, the PS approach led to higher levels of contaminants, including apolipoproteins and highly abundant secreted plasma proteins compared to UC2. Furthermore, annexin family members and many ECM-associated proteins were found specifically enriched in plasma EVPs isolated using PS, likely a consequence of the high Ca^{2+} concentration in the experimental condition, which modulates the molecular interactions of annexins and several ECM and ECM-associated proteins.

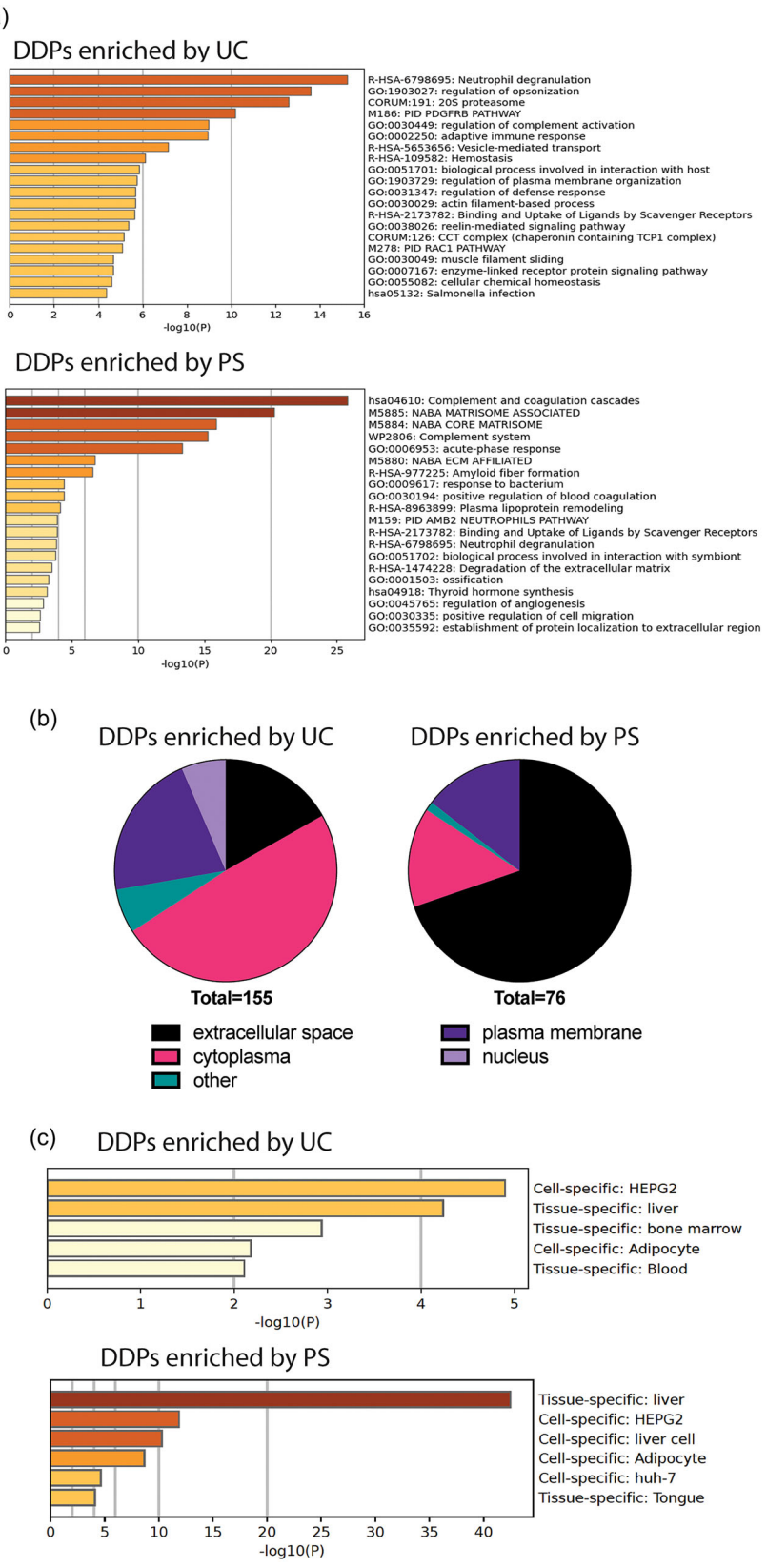

FIGURE 4 Distinct proteomic compositions of plasma EVPs isolated through PS and UC-based approaches. (a) Metascape analysis of top pathways associated with DDPs enriched by UC-based approaches (top panel) and PS (bottom panel), respectively. (b) Subcellular localization analysis of DDPs enriched by UC-based approaches (left chart) and PS (right chart), respectively. (c) Enrichment analysis of tissue- and cell-specific pattern genes in DDPs enriched by UC-based approaches (top panel) and PS (bottom panel), respectively.

Our findings underscore the heterogeneity of plasma EVPs and the potential for isolation bias toward certain EVP subsets through different isolation procedures. Therefore, it is crucial to utilize consistent sample handling procedures and conditions for studies cross-comparing and validating plasma EVP biomarkers. Various factors, such as the type of anticoagulants used for plasma preparation and the concentrations of calcium and other ions in the buffer, can influence molecular interactions and thus affect the proteomic constitution of the isolated EVPs and study outcomes. Hence, careful consideration of these variables should be taken into account when designing and interpreting experiments involving plasma EVPs.

It is important to note that the choice of EVP isolation strategy should be based on the research question, experimental goals, and the specific characteristics and heterogeneity of the EVPs being studied. In the present work, we focused on evaluating the performance of different procedures for improving the purity of plasma EVP isolation for downstream proteomic profiling via MS, which is critical for biomarker discovery. However, the choice of EVP isolation strategy should be tailored to the nature of the samples (e.g., plasma, cell culture, or tissue) and the endpoint assays, which may present specific requirements for the purity, quantity, and functionality preservation of isolated EVPs. Therefore, it is important to carefully consider the trade-offs between the isolation efficiency, purity, and the preservation of the biological properties of the isolated EVPs, and choose a suitable isolation method accordingly.

Our study shows that UC3 and UC2-qEV improve EVP purity but at the expense of yield. However, whereas UC2-qEV requires a larger input plasma volume, UC3 can typically provide sufficient material for downstream proteomic analysis using 2–5 mL of plasma, making it suitable for most clinical scenarios. We also found that frozen plasma UC2 samples can be further purified by adding one UC washing step to achieve better EVP purity and enable further in-depth proteomic profiling, although the total yield is compromised compared to samples freshly processed via UC3 (data not shown). This allows us to further purify previously banked patient plasma EVP samples. Furthermore, both UC-based modified procedures only require an ultracentrifuge and no specific isolating platforms or instruments, making them readily adapted by most research and clinical laboratories conducting biomarker discovery studies involving large cohorts of patient samples. Once biomarkers are identified, more user-friendly and scalable methods should be developed to allow for automation, facilitating high-throughput processing, and routine clinical implementation.

Lastly, while this study reports on a modified procedure to improve plasma EVP purity and the depth of proteomic profiling, it is important to highlight the potential loss of certain subsets that can occur when the recovery rate is compromised in pursuit of higher purity. To mitigate this issue, employing multiple strategies for circulating EVP isolation and characterization in large cohort studies can be beneficial. These complementary approaches can enhance the potential for biomarker discovery.

AUTHOR CONTRIBUTIONS

Zurong Wan: Conceptualization; data curation; formal analysis; investigation; methodology; writing—original draft; writing—review and editing. **Jinghua Gu**: Formal analysis; methodology; writing—review and editing. **Uthra Balaji**: Formal analysis. **Linda Bojmar**: Data curation; investigation; writing—review and editing. **Henrik Molina**: Resources; software. **Søren Heissel**: Resources; software. **Alexandra E. Pagano**: Resources; software. **Christopher Peralta**: Resources; software. **Lee Shaashua**: Formal analysis. **Dorina Ismailgeci**: Data curation. **Hope K. Narozniak**: Data curation. **Yi Song**: Data curation. **William R. Jarnagin**: Data curation; writing—review and editing. **David P. Kelsen**: Data curation; writing—review and editing. **Jaqueline Bromberg**: Investigation; writing—review and editing. **Virginia Pascual**: Conceptualization; formal analysis; funding acquisition; investigation; supervision; writing—review and editing. **Haiying Zhang**: Conceptualization; formal analysis; funding acquisition; investigation; methodology; supervision; writing—original draft; writing—review and editing.

ACKNOWLEDGEMENTS

The authors thank colleagues David Lyden, Irina Matei, Candia Kenific, Nancy Boudreau, Larry Remmel, and Katia Manova for their feedback on the project and reading the manuscript. The authors gratefully acknowledge support from the National Cancer Institute (CA232093, CA163117, CA224175, CA163120, CA169538, CA210240, CA207983 and AI144301 (NIAID) to David Lyden, and CA218513 to David Lyden and Haiying Zhang), the Thompson Family Foundation (to David Lyden), the Tortolani Foundation (to David Lyden), the Pediatric Oncology Experimental Therapeutics Investigator's Consortium, the Malcolm Hewitt Weiner Foundation, the Manning Foundation, the Sohn Foundation, the Theodore A. Rapp Foundation, the Hartwell Foundation, the AHEPA Vth District Cancer Research Foundation, Alex's Lemonade Stand Foundation, the Breast Cancer Research Foundation, the Feldstein Medical Foundation, the Tortolani Foundation, the Daedalus Fund Selma and Lawrence Ruben Science to Industry Bridge Award, and the Children's Cancer and Blood Foundation (all to David Lyden), the Swedish Cancer Society project grant (21 1824 Pj 01 H to Linda Bojmar), the Swedish Research Society Starting Grant (2021-02356 to Linda Bojmar), the Swedish Society for Medical Research (S21-0079, to Linda Bojmar), the National Institute of Allergy and Infectious Diseases (AI144301, to Virginia Pascual), the Drukier Institute for Children's Health at Weill Cornell Medicine (to Virginia Pascual), Sohn Conferences Foundation and the Leona M. and Harry B. Helmsley Charitable Trust (to Proteomics Resource Center at The Rockefeller University).

CONFLICT OF INTEREST STATEMENT

The authors declare conflicts of interest.

ORCID

Haiying Zhang https://orcid.org/0000-0002-7158-2373

REFERENCES

Arraud, N., Linares, R., Tan, S., Gounou, C., Pasquet, J. M., Mornet, S., & Brisson, A. R. (2014). Extracellular vesicles from blood plasma: Determination of their morphology, size, phenotype and concentration. *Journal of Thrombosis and Haemostasis*, *12*(5), 614–627. https://doi.org/10.1111/jth.12554

Camont, L., Lhomme, M., Rached, F., Le Goff, W., Negre-Salvayre, A., Salvayre, R., Calzada, C., Lagarde, M., Chapman, M. J., & Kontush, A. (2013). Small, dense high-density lipoprotein-3 particles are enriched in negatively charged phospholipids: Relevance to cellular cholesterol efflux, antioxidative, antithrombotic, anti-inflammatory, and antiapoptotic functionalities. *Arteriosclerosis Thrombosis and Vascular Biology*, *33*(12), 2715–2723. https://doi.org/10.1161/ATVBAHA.113.301468

Chen, G. Y., Cheng, J. C., Chen, Y. F., Yang, J. C., & Hsu, F. M. (2021). Circulating exosomal integrin beta3 is associated with intracranial failure and survival in lung cancer patients receiving cranial irradiation for brain metastases: A prospective observational study. *Cancers (Basel)*, *13*(3), 380. https://doi.org/10.3390/cancers13030380

Chen, I. H., Xue, L., Hsu, C. C., Paez, J. S., Pan, L., Andaluz, H., Wendt, M. K., Iliuk, A. B., Zhu, J. K., & Tao, W. A. (2017). Phosphoproteins in extracellular vesicles as candidate markers for breast cancer. *Proceedings of National Academy of Science USA*, *114*(12), 3175–3180. https://doi.org/10.1073/pnas.1618088114

Choi, D. S., Kim, D. K., Kim, Y. K., & Gho, Y. S. (2015). Proteomics of extracellular vesicles: Exosomes and ectosomes. *Mass Spectrometry Reviews*, *34*(4), 474–490. https://doi.org/10.1002/mas.21420

Clayton, A., Turkes, A., Dewitt, S., Steadman, R., Mason, M. D., & Hallett, M. B. (2004). Adhesion and signaling by B cell-derived exosomes: the role of integrins. *FASEB Journal*, *18*(9), 977–979. https://doi.org/10.1096/fj.03-1094fje

Colombo, M., Raposo, G., & Thery, C. (2014). Biogenesis, secretion, and intercellular interactions of exosomes and other extracellular vesicles. *Annual Review of Cell and Developmental Biology*, *30*, 255–289. https://doi.org/10.1146/annurev-cellbio-101512-122326

Corso, G., Mager, I., Lee, Y., Gorgens, A., Bultema, J., Giebel, B., Wood, M. J. A., Nordin, J. Z., & Andaloussi, S. E. (2017). Reproducible and scalable purification of extracellular vesicles using combined bind-elute and size exclusion chromatography. *Science Reports*, *7*(1), 11561. https://doi.org/10.1038/s41598-017-10646-x

Fraser, K., Jo, A., Giedt, J., Vinegoni, C., Yang, K. S., Peruzzi, P., Chiocca, E. A., Breakefield, X. O., Lee, H., & Weissleder, R. (2019). Characterization of single microvesicles in plasma from glioblastoma patients. *Neuro Oncology*, *21*(5), 606–615. https://doi.org/10.1093/neuonc/noy187

Hoshino, A., Costa-Silva, B., Shen, T. L., Rodrigues, G., Hashimoto, A., Tesic Mark, M., Molina, H., Kohsaka, S., Di Giannatale, A., Ceder, S., Singh, S., Williams, C., Soplop, N., Uryu, K., Pharmer, L., King, T., Bojmar, L., Davies, A. E., Ararso, Y., … Lyden, D. (2015). Tumour exosome integrins determine organotropic metastasis. *Nature*, *527*(7578), 329–335. https://doi.org/10.1038/nature15756

Hoshino, A., Kim, H. S., Bojmar, L., Gyan, K. E., Cioffi, M., Hernandez, J., Zambirinis, C. P., Rodrigues, G., Molina, H., Heissel, S., Mark, M. T., Steiner, L., Benito-Martin, A., Lucotti, S., Di Giannatale, A., Offer, K., Nakajima, M., Williams, C., Nogués, L., … Lyden, D. (2020). Extracellular vesicle and particle biomarkers define multiple human cancers. *Cell*, *182*(4), 1044–1061e1018. https://doi.org/10.1016/j.cell.2020.07.009

Hsu, C. Y., Hsieh, T. H., Lin, H. Y., Lu, C. Y., Lo, H. W., Tsai, C. C., & Tsai, E. M. (2021). Characterization and proteomic analysis of endometrial stromal cell-derived small extracellular vesicles. *Journal of Clinical Endocrinology and Metabolism*, *106*(5), 1516–1529. https://doi.org/10.1210/clinem/dgab045

Kalra, H., Simpson, R. J., Ji, H., Aikawa, E., Altevogt, P., Askenase, P., Bond, V. C., Borràs, F. E., Breakefield, X., Budnik, V., Buzas, E., Camussi, G., Clayton, A., Cocucci, E., Falcon-Perez, J. M., Gabrielsson, S., Gho, Y. S., Gupta, D., Harsha, H. C., … Mathivanan, S. (2012). Vesiclepedia: a compendium for extracellular vesicles with continuous community annotation. *PLoS Biology*, *10*(12), e1001450. https://doi.org/10.1371/journal.pbio.1001450

Keklikoglou, I., Cianciaruso, C., Guc, E., Squadrito, M. L., Spring, L. M., Tazzyman, S., Lambein, L., Poissonnier, A., Ferraro, G. B., Baer, C., Cassará, A., Guichard, A., Iruela-Arispe, M. L., Lewis, C. E., Coussens, L. M., Bardia, A., Jain, R. K., Pollard, J. W., & De Palma, M. (2019). Chemotherapy elicits pro-metastatic extracellular vesicles in breast cancer models. *Nature Cell Biology*, *21*(2), 190–202. https://doi.org/10.1038/s41556-018-0256-3

Kim, D. K., Lee, J., Simpson, R. J., Lotvall, J., & Gho, Y. S. (2015). EVpedia: A community web resource for prokaryotic and eukaryotic extracellular vesicles research. *Seminars in Cell and Developmental Biology*, *40*, 4–7. https://doi.org/10.1016/j.semcdb.2015.02.005

Ko, J., Bhagwat, N., Black, T., Yee, S. S., Na, Y. J., Fisher, S., Kim, J., Carpenter, E. L., Stanger, B. Z., & Issadore, D. (2018). miRNA profiling of magnetic nanopore-isolated extracellular vesicles for the diagnosis of pancreatic cancer. *Cancer Research*, *78*(13), 3688–3697. https://doi.org/10.1158/0008-5472.CAN-17-3703

Leoni, G., Neumann, P. A., Kamaly, N., Quiros, M., Nishio, H., Jones, H. R., Sumagin, R., Hilgarth, R. S., Alam, A., Fredman, G., Argyris, I., Rijcken, E., Kusters, D., Reutelingsperger, C., Perretti, M., Parkos, C. A., Farokhzad, O. C., Neish, A. S., & Nusrat, A. (2015). Annexin A1-containing extracellular vesicles and polymeric nanoparticles promote epithelial wound repair. *Journal of Clinical Investigation*, *125*(3), 1215–1227. https://doi.org/10.1172/JCI76693

Lucotti, S., Kenific, C. M., Zhang, H., & Lyden, D. (2022). Extracellular vesicles and particles impact the systemic landscape of cancer. *EMBO Journal*, *41*(18), e109288. https://doi.org/10.15252/embj.2021109288

Maji, S., Chaudhary, P., Akopova, I., Nguyen, P. M., Hare, R. J., Gryczynski, I., & Vishwanatha, J. K. (2017). Exosomal Annexin II promotes angiogenesis and breast cancer metastasis. *Molecular Cancer Research*, *15*(1), 93–105. https://doi.org/10.1158/1541-7786.MCR-16-0163

Mathivanan, S., & Simpson, R. J. (2009). ExoCarta: A compendium of exosomal proteins and RNA. *Proteomics*, *9*(21), 4997–5000. https://doi.org/10.1002/pmic.200900351

Pan, J. B., Hu, S. C., Shi, D., Cai, M. C., Li, Y. B., Zou, Q., & Ji, Z. L. (2013). PaGenBase: A pattern gene database for the global and dynamic understanding of gene function. *PLoS ONE*, *8*(12), e80747. https://doi.org/10.1371/journal.pone.0080747

Park, E. J., Prajuabjinda, O., Soe, Z. Y., Darkwah, S., Appiah, M. G., Kawamoto, E., Momose, F., Shiku, H., & Shimaoka, M. (2019). Exosomal regulation of lymphocyte homing to the gut. *Blood Advances*, *3*(1), 1–11. https://doi.org/10.1182/bloodadvances.2018024877

Pelissier Vatter, F. A., Cioffi, M., Hanna, S. J., Castarede, I., Caielli, S., Pascual, V., Matei, I., & Lyden, D. (2021). Extracellular vesicle- and particle-mediated communication shapes innate and adaptive immune responses. *Journal of Experimental Medicine*, *218*(8), e20202579. https://doi.org/10.1084/jem.20202579

Perkins, D. N., Pappin, D. J., Creasy, D. M., & Cottrell, J. S. (1999). Probability-based protein identification by searching sequence databases using mass spectrometry data. *Electrophoresis*, *20*(18), 3551–3567. https://doi.org/10.1002/(SICI)1522-2683(19991201)20:18⟨3551::AID-ELPS3551⟩3.0.CO;2-2

R Core Team. (2021). R: A Language and Environment for Statistical Computing. Retrieved from https://www.R-project.org/

Ritchie, M. E., Phipson, B., Wu, D., Hu, Y., Law, C. W., Shi, W., & Smyth, G. K. (2015). limma powers differential expression analyses for RNA-sequencing and microarray studies. *Nucleic Acids Research*, *43*(7), e47. https://doi.org/10.1093/nar/gkv007

Sheehan, C., & D'Souza-Schorey, C. (2019). Tumor-derived extracellular vesicles: Molecular parcels that enable regulation of the immune response in cancer. *Journal of Cell Science*, *132*(20), jcs235085. https://doi.org/10.1242/jcs.235085

Shimada, Y., Matsubayashi, J., Kudo, Y., Maehara, S., Takeuchi, S., Hagiwara, M., Kakihana, M., Ohira, T., Nagao, T., & Ikeda, N. (2021). Serum-derived exosomal PD-L1 expression to predict anti-PD-1 response and in patients with non-small cell lung cancer. *Scientific Reports*, *11*(1), 7830. https://doi.org/10.1038/s41598-021-87575-3

Simonsen, J. B. (2017). What Are We Looking At? Extracellular Vesicles, Lipoproteins, or Both? *Circulation Research*, *121*(8), 920–922. https://doi.org/10.1161/CIRCRESAHA.117.311767

Trefts, E., Gannon, M., & Wasserman, D. H. (2017). The liver. *Current Biology*, *27*(21), R1147–R1151. https://doi.org/10.1016/j.cub.2017.09.019

Vergauwen, G., Tulkens, J., Pinheiro, C., Avila Cobos, F., Dedeyne, S., De Scheerder, M. A., Vandekerckhove, L., Impens, F., Miinalainen, I., Braems, G., Gevaert, K., Mestdagh, P., Vandesompele, J., Denys, H., De Wever, O., & Hendrix, A. (2021). Robust sequential biophysical fractionation of blood plasma to study variations in the biomolecular landscape of systemically circulating extracellular vesicles across clinical conditions. *Journal of Extracellular Vesicles*, *10*(10), e12122. https://doi.org/10.1002/jev2.12122

Xu, R., Rai, A., Chen, M., Suwakulsiri, W., Greening, D. W., & Simpson, R. J. (2018). Extracellular vesicles in cancer—implications for future improvements in cancer care. *Nature Reviews in Clinical Oncology*, *15*(10), 617–638. https://doi.org/10.1038/s41571-018-0036-9

Zhang, H., Freitas, D., Kim, H. S., Fabijanic, K., Li, Z., Chen, H., Mark, M. T., Molina, H., Martin, A. B., Bojmar, L., Fang, J., Rampersaud, S., Hoshino, A., Matei, I., Kenific, C. M., Nakajima, M., Mutvei, A. P., Sansone, P., Buehring, W., … Lyden, D. (2018). Identification of distinct nanoparticles and subsets of extracellular vesicles by asymmetric flow field-flow fractionation. *Nature Cell Biology*, *20*(3), 332–343. https://doi.org/10.1038/s41556-018-0040-4

Zhang, X., Smits, A. H., van Tilburg, G. B., Ovaa, H., Huber, W., & Vermeulen, M. (2018). Proteome-wide identification of ubiquitin interactions using UbIA-MS. *Nature Protocols*, *13*(3), 530–550. https://doi.org/10.1038/nprot.2017.147

SUPPORTING INFORMATION

Additional supporting information can be found online in the Supporting Information section at the end of this article.

How to cite this article: Wan, Z., Gu, J., Balaji, U., Bojmar, L., Molina, H., Heissel, S., Pagano, A. E., Peralta, C., Shaashua, L., Ismailgeci, D., Narozniak, H. K., Song, Y., Jarnagin, W. R., Kelsen, D. P., Bromberg, J., Pascual, V., & Zhang, H. (2024). Optimization of ultracentrifugation-based method to enhance the purity and proteomic profiling depth of plasma-derived extracellular vesicles and particles. *Journal of Extracellular Biology*, *3*, e167. https://doi.org/10.1002/jex2.167